LA-UR -91-109

Los Alamos National Laboratory is operated by the University of California for the United States Department of Energy under contract W-7405-ENG-36

LA-UR--91-109

DE91 007384

TITLE: LOW-FREQUENCY COMPUTATIONAL ELECTROMAGNETICS FOR ANTENNA ANALYSIS

AUTHOR(S): E. K. Miller and G. J. Burke

SUBMITTED TO: Proc. IEEE '91

DISCLAIMER

Los Alamos Los Alamos National Laboratory
Los Alamos, New Mexico 87545

FORM NO 836 R4
ST NO 2629 5/81

LOW-FREQUENCY COMPUTATIONAL ELECTROMAGNETICS FOR ANTENNA ANALYSIS

E. K. Miller, Group MEE-3, MS J580
Los Alamos National Laboratory
PO Box 1663, Los Alamos, NM 87545

G. J. Burke, L-156
Lawrence Livermore National Laboratory
PO Box 808, Livermore, CA 94550

ABSTRACT

An overview of low-frequency, compuational methods for modeling the electromagnetic characteristics of antennas is presented here. The article presents a brief analytical background, and summarizes the essential ingredients of the method of moments, for numerically solving low-frequency antenna problems. Some extensions to the basic models of perfectly conducting objects in free space are also summarized, followed by a consideration of some of the some computational issues that affect model accuracy, efficiency and utility. A variety of representative computations are then presented to illustrate various modeling aspects and capabilities that are currently available. A fairly extensive bibliography is included to suggest further reference material to the reader.

1. INTRODUCTION

Although Computational ElectroMagnetics (CEM) dates its origin prior to development of the large-scale digital computer, depending previously on mechanical calculators for the necessary computations, it truly began in the early 1960s with the appearance of the first scientific mainframes. With the approximately 10,000,000 times speed increase from the 1,000 floating-point operations (FLOPs)/second of the UNIVAC-1 to the near-10 GigaFLOP speed of the present mainframes, the size, complexity and scope of problems that are routinely computer modeled not only in electromagnetics but in all of science and engineering, has vastly increased. The purpose of this article is to summarize present capabilities in CEM for antenna applications.

The article title includes the words "low frequency" because in spite of the continuing increase in computer speed that is occurring, a factor of 10 about every five years, the raw "number-crunching" requirements of first-principles, numerically-rigorous EM modeling grows at least as fast as the fourth power of the frequency, f, for a given problem. Thus, it is not hard to challenge the capacity of 10 GigaFLOP computers, and when the speed has further increased to 1 TeraFLOP or 1 PetaFLOP, the set of problems for which computer modeling is practical will be less dramatically expanded. The digital computer has never-the-less irrevocably altered the world of the electromagneticest, supplementing and complementing analysis and measurement with computer modeling as a third method of problem solving.

The article is organized as follows. In Section 2 we present the necessary analytical background to explain the mathematically formal descriptions of low-frequency antenna models that are included here. This is followed in Section 3 by a summary of the numerical treatments employed to obtain quantitative results from the analytical descriptions. We consider some extensions to the basic problem of perfect condutors in free space in Section 4, followed by a consideration of some computational issues that affect model selection and application in Section 5. A survey of representative modeling capabilities and applications is included in Section 6, with some concluding Section comments in Section 7.

2. ANALYTICAL BACKGROUND

As already discussed by Balanis in the first paper in this issue [1], the analytical starting point for electromagnetics is Maxwell's Equations. These equations can be expressed in two distinctly different forms. Perhaps most familiar is their differential form, when they are written as curl and divergence relations. An alternate way of writing Maxwell's Equations is in a source-integral form using some appropriate Green's function, usually that for an infinite medium. The essential difference between these two descriptions of electromagnetic fields, and other formulations such as the geometrical theory of diffraction and modal expansions based on multipoles, arises from the analytical means by which source-field relationships are prescribed, i.e., in how field "propagation" is described mathematically. In addition, these equations can be written in the time domain with time an explicit, independent variable, or in the frequency domain for a radian frequency ω where a time variation of the form $e^{j\omega t}$ is assumed.

Numerical models can be developed using either form and either domain. Those derived from the differential equations are usually called finite-difference and finite-element models, while those based on integral equations are known as boundary-element or moment-method models, about which more discussion follows in Section 3 below. For convenience, we use the abbreviations DE and IE to denote differential-equation and integral-equation models, and FD and TD similarly to indicate whether they are formulated in the frequency domain or time domain. Thus, TDDE is used for a differential-equation model developed in the time domain.

2.1 Maxwell's Equations and the Wave Equation

For infinite, homogeneous, isotropic media, Maxwell equations in the TD as a function of space coordinate $\mathbf{r}$ and time t are given by [2]

$$\nabla\times\mathbf{E}(\mathbf{r},t) = -\mu\frac{\partial}{\partial t}\mathbf{H}(\mathbf{r},t) - \mathbf{K}(\mathbf{r},t), \qquad \nabla\cdot\mathbf{E}(\mathbf{r},t) = \rho(\mathbf{r},t)/\varepsilon,$$

$$\nabla\times\mathbf{H}(\mathbf{r},t) = \varepsilon\frac{\partial}{\partial t}\mathbf{E}(\mathbf{r},t) + \mathbf{J}(\mathbf{r},t), \qquad \nabla\cdot\mathbf{H}(\mathbf{r},t) = m(\mathbf{r},t)/\mu, \tag{1}$$

with $\mathbf{E}(\mathbf{r},t)$ and $\mathbf{H}(\mathbf{r},t)$ the space- and time-dependent electric and magnetic field vectors, $\mathbf{J}(\mathbf{r},t)$ and $\mathbf{K}(\mathbf{r},t)$ the electric and magnetic current densities, $\rho(\mathbf{r},t)$ and $m(\mathbf{r},t)$ the

electric and magnetic charge densities, and ε and μ the medium electric permittivity and magnetic permeability. Their FD counterparts are obtained from (1) by separating time and space variables, i.e. using $F(x,t) \equiv f(x,\omega)e^{j\omega t}$, which replaces the time derivatives by $j\omega$ multipliers. The TD wave equation for $\mathbf{E}(\mathbf{r},t)$ can be derived from (1) to obtain

$$\nabla\times\nabla\times\mathbf{E}(\mathbf{r},t) + \frac{1}{c^2}\frac{\partial^2}{\partial t^2}\mathbf{E}(\mathbf{r},t) = -\mu\frac{\partial}{\partial t}\mathbf{J}(\mathbf{r},t) - \nabla\times\mathbf{K}(\mathbf{r},t) \tag{3}$$

with a similar equation for $\mathbf{H}(\mathbf{r},t)$, where $c = 1/\sqrt{\mu\varepsilon}$ is the speed of light in the medium.

2.2 Green's Function Representation of Maxwell's Equations

DEs of the kind above can be readily solved for point current sources [3], in terms of the infinite, homogeneous medium, scalar Green's functions $\varphi_t(\mathbf{r},\mathbf{r}',t,t') = \delta(t-R/c-t')/R$ and $\varphi_\omega(\mathbf{r},\mathbf{r}',\omega) = e^{-ikR}/R$, respectively, where $R = |\mathbf{r} - \mathbf{r}'|$ is the distance separating a source at $\mathbf{r}'$ and observation point at $\mathbf{r}$, the wavenumber $k = \omega/c$, and $t' = t - R/c$ is the retarded time. Additional vector-differential operations on these Green's functions then yield the various time- and frequency-dependent field components as a dyadic Green's function [4], which for electric currents in the FD is given by $-j\omega\mu(k^2\mathbf{I} + \nabla\nabla)/k^2$ with $\mathbf{I}$ the unit dyadic. It should be noted that the only condition satisfied by the fields obtained in this manner is the Sommerfeld radiation condition [2], which means that their outward propagating components, in the FD, satisfy the condition $(\mathbf{r}\cdot\nabla + jk)f(\mathbf{r},\omega) = 0$ as $|\mathbf{r}| \dashrightarrow \infty$, i.e., their phase advances with increasing distance from the source and they attenuate as 1/R.

Using the superposition principle, we are then able to represent the electromagnetic fields as an integral of the dyadic Green's function operating on an arbitrary source distribution. The sources could be volumetric distributions of free charges and currents, or the tangential components of the fields produced by these sources over a surface that encloses them. Alternatively, the sources could reside on surfaces separating two electrically dissimilar media, such as a perfect conductor and free space. We are thus able to derive Green's-function integral representations of the total field in the FD, as

$$\mathbf{E}(\mathbf{r}) = T\mathbf{E}^{inc}(\mathbf{r}) - \frac{T}{4\pi}\int_S \{j\omega\mu(\mathbf{n}'\times\mathbf{H})\varphi_\omega - (\mathbf{n}'\times\mathbf{E})\times\nabla'\varphi_\omega - (\mathbf{n}'\cdot\mathbf{E})\nabla'\varphi_\omega\}ds' \tag{3a}$$

and

$$\mathbf{H}(\mathbf{r}) = T\mathbf{H}^{inc}(\mathbf{r}) + \frac{T}{4\pi}\int_S \{j\omega\varepsilon(\mathbf{n}'\times\mathbf{E})\varphi_\omega + (\mathbf{n}'\times\mathbf{H})\times\nabla'\varphi_\omega + (\mathbf{n}'\cdot\mathbf{H})\nabla'\varphi_\omega\}ds' \tag{3b}$$

where **n** is an outward-pointing unit vector normal to S and the quantity $T = (1 - \Omega/4\pi)^{-1}$ permits the observation point in (3) to be located outside or on the surface S [5]. Similar integral expressions can be derived in the TD, which are omitted for brevity. We see that, were the sources on the surface S to be known, the fields would then be completely determinable, but since that is not the case, our problem has now become one of finding *that* source distribution on a prescribed surface whose fields, together with the incident field causing those sources, will satisfy the required boundary conditions. This is the basic idea behind the need for solving an integral equation, whose derivation is next discussed.

2.3 Developing an Integral Equation

Derivation of an IE from integral expressions for the fields as given above can be achieved in various ways. One of the most appealing on physical grounds, though involving some mathematically challenging issues such as singular integrals, is boundary-condition matching. That is, we can let the observation point in (3) approach a surface on which the total field satisfies known boundary conditions. At the surface of a penetrable object, for example, the tangential components of both the electric and magnetic fields are known to be continuous. If the object in question is a perfect electric conductor, the situation most commonly encountered in antenna analysis and design, then the total tangential electric field is zero,or $\mathbf{n}\times[\mathbf{E}^{scat}(\mathbf{r}) + \mathbf{E}^{inc}(\mathbf{r})] = 0$, with $\mathbf{E}^{scat}(\mathbf{r})$ being the field of the sources caused by the incident field. Two different kinds of IEs can be derived for perfect conductors from (4), having either the incident electric field or incident magnetic field as the forcing function. The IEs for penetrable objects involve both field components together.

2.3.1 Frequency-Domain Integral Equations--For a perfectly

conducting object defined by the surface S, (4) reduces to the following IEs:

$$\mathbf{n}\times\mathbf{E}^{inc}(\mathbf{r}) = \frac{1}{4\pi}\mathbf{n}\times\int_S \left\{ j\omega\mu\mathbf{J}\varphi_\omega + \frac{1}{j\omega}(\nabla\cdot\mathbf{J})\nabla'\varphi_\omega \right\} ds',\ \mathbf{r}\in S, \tag{4a}$$

and

$$\mathbf{J}(\mathbf{r}) = 2\mathbf{n}\times\mathbf{H}^{inc}(\mathbf{r}) + \frac{1}{2\pi}\mathbf{n}\times\int_S \mathbf{J}\times\nabla'\varphi_\omega ds',\ \mathbf{r}\in S. \tag{4b}$$

where $\mathbf{J} = \mathbf{n}\times\mathbf{H}$ is the surface current on the conducting body. Equation (4a) is known as the electric-field integral equation (EFIE) and (4b) as the magnetic-field integral equation (MFIE). They are Fredholm IEs of the first and second kinds respectively, in which the unknown appears either only under the integral sign, or outside it as well. The mathematical operations on the unknown which occur under the integral sign are called the "kernel" of the integral equation. In terms of applicability, the EFIE is suited to more general object shapes, including thin plates, open shells and wires, while the MFIE's applicability is limited to closed, relatively smooth, objects.

2.3.2 Time-Domain Integral Equations--Equivalent TDIEs are given by

$$\mathbf{n}\times\mathbf{E}^{inc}(\mathbf{r},t) = \frac{1}{4\pi}\mathbf{n}\times\int_S \left[\mu\frac{\partial}{\partial t'}\mathbf{J}_s(\mathbf{r}',t')\frac{1}{|\mathbf{r}-\mathbf{r}'|} - \left(\frac{1}{|\mathbf{r}-\mathbf{r}'|} + \frac{1}{c}\frac{\partial}{\partial t'}\right)\frac{\rho_s(s',t')}{\varepsilon}\frac{\mathbf{r}-\mathbf{r}'}{|\mathbf{r}-\mathbf{r}'|^2} \right] da' \tag{5a}$$

and

$$\mathbf{J}(\mathbf{r},t) = 2\mathbf{n}\times\mathbf{H}^{inc}(r,t) + \frac{1}{2\pi}\int_S \mathbf{n}\times\left\{ \left[\frac{1}{R} + \frac{1}{c}\frac{\partial}{\partial t'} \right]\mathbf{J}(\mathbf{r}',t')\times\frac{\mathbf{R}}{R^2} \right\} da' \tag{5b}$$

respectively, where the surface-charge density, ρ_S, comes from the integral form of the continuity equation

$$\rho_s(s,t) = -\int_{-\infty}^{t} \nabla\cdot\mathbf{J}(s,\tau)d\tau$$

2.4 Integral Equations for Wires

Wires are a special class of objects whose study has long occupied electromagneticests. This is because much of the early development of radio-wave

communication incorporated wires and wirelike objects as antennas. In addition, thin wires also represented one of the few geometries beyond those admitting separation-of-variables solutions, such as circular cylinders and spheres, amenable to analysis prior to the digital computer [6]. Finally, when arranged to form a mesh, more general conducting bodies can be approximated both physically and mathematically, by collections of wires. Several kinds of IEs have been used for wires, in both the TD and FD. Some of the more commonly-used ones are summarized below.

2.4.1 Frequency-Domain IEs for Wires--In the context of the thin-wire approximation (TWA), a wire is represented as a circular cylinder of diameter D and length L such that $D \ll L$ and $D \ll \lambda$, about which several assumptions are made. First, it is assumed that the azimuthally-directed component of surface current is negligible. Second, the longitudinally flowing current, I(s'), is taken to be independent of azimuth. Finally, because only the longitudinal electric field is then important, the boundary condition is enforced on only this field component and the surface integrals are simplified to one-dimensional line integrals using the so-called reduced kernel in the IE. More details on the TWA and its implementation can be found in [7] and [8].

Perhaps the oldest wire IE is that derived by Pocklington [5] for a straight wire, whose more general form is expressed by

$$\mathbf{s}\cdot\mathbf{E}^{inc}(s) = -\frac{1}{4\pi j\omega\varepsilon}\int_{C(r)} I(s')\left[k^2\mathbf{s}\cdot\mathbf{s}' - \frac{\partial}{\partial s}\frac{\partial}{\partial s'}\right]\frac{e^{-jkR}}{R}ds',\ s\in C(\mathbf{r}) \tag{6}$$

where $\mathbf{s}$ and $\mathbf{s}'$ are unit tangent vectors to the wire at s and s' respectively, and $C(\mathbf{r})$ defines the wire geometry with s displaced by the wire radius a from the source filament at s'. Other versions of the TWA IE are the mixed-potential form [1] and the generalized Hallen IE [9].

2.4.2 Time-Domain IE for Wires --Equivalent TD versions of the FDIEs for wires can also be developed. One example is given by [10]

$$\mathbf{s}\cdot\mathbf{E}^{inc}(s,t) = \frac{\mu_0}{4\pi}\int_{C(r)}\left[\frac{\mathbf{s}\cdot\mathbf{s}'}{R}\frac{\partial}{\partial t'}I(s',t') + c\frac{\mathbf{s}\cdot\mathbf{R}}{R^2}\frac{\partial}{\partial s'}I(s',t') - c^2\frac{\mathbf{s}\cdot\mathbf{R}}{R^3}q(s',t')\right]ds',\ s\in C(\mathbf{r}) \tag{7}$$

2.5 Operator Form of the Equations

It is convenient to express the various equations summarized here, both differential as in (1) and integral as in (4), (5), (6) and (7), more concisely for subsequent discussion of their numerical treatment using the MM. In the FD, following Harrington [11], we use the generic operator form

$$L(s,s';\omega)f(s';\omega) = g(s;\omega) \Rightarrow L(s,s')f(s') = g(s) \tag{8}$$

where the explicit dependence on frequency is normally suppressed. In this shorthand notation, L(s,s') represents an integral or differential operator, f(s') is the unknown, and g(s) is the forcing function, or "right-hand side" (RHS) of the equation. A similar expression can be written for the TD as

$$L(s,s';t,t')f(s';t') = g(s;t) \tag{9}$$

where the explicit dependence on source and observation times is retained to distinguish this equation from its FD counterpart.

It should be noted that the formulation and numerical solution via the MM, as briefly outlined below, is independent of the RHS, so that most models are equally applicable to radiation or scattering problems. For the former, the RHS is a localized "incident field," usually a voltage or a specified tangential electric or magnetic field defined over a limited region of the model. In the latter case, the incident field exists over the entire structure being modeled. Therefore, although this discussion is specifically addressed to low-frequency antenna modeling, we include a number of references to scattering applications.

3. NUMERICAL TREATMENT

Although the term "moment method" (MM) has come to be most commonly associated with integral-equation models, it actually refers to a general procedure for numerically solving DE, IE and integro-differential equations in the TD and FD [11]. The MM is an intuitively logical way to develop a numerical solution to equations of these kinds. Its basic steps are generically the same whatever the specific kind of equation is being solved. These are first briefly outlined below, and then described more completely in the following sections.

3.1 The Basic Steps in the MM for the Frequency Domain

1) *Sampling* and *approximating* the unknown sources and/or fields whose solutions are sought using some appropriate *basis-* or *expansion* -function representation, involving unknown constants whose numerical solution is the goal of the MM model.

2) *Sampling* the defining equations which the expansion-function representation is required to satisfy in a manner determined by some *weighting* or *testing* functions, to develop quantitative relationships among the unknown constants and thereby forming a *linear system of equations*.

3) *Solving* the linear system of equations using various matrix procedures.

3.2 Time-Stepping for a Solution in the Time Domain

Developing a MM model from a TD formulation requires not only space sampling, but also involves:

4) Developing a time response using *time sampling and stepping*.

3.3 Further Consideration of the Moment Method

3.3.1 *Sampling* and *approximating* the unknown sources/fields--

Two basically different kinds of expansions can be used. One is the *entire-domain* basis (EDB) which is defined over the entire object or space being modeled, an example being the Fourier series $\sum I_n \sin(2\pi ns/L)$, n = 1,. . . , to represent the current on a wire or two-dimensional strip. For a general object whose surface is defined by G(**r**), the EDB can be expressed as

$$f(s') = \sum_{i=1}^{X_S} I_i b_i(s'),\ s' \in G(\mathbf{r}) \qquad (10$$

where there are X_S unknown coefficients I_i whose quantitative values are to be obtained in the MM solution and the $b_i(s')$ are the basis functions.

Although useful for simpler objects, EDB are not as well suited for more complex geometries such as aircraft, for example, for which *sub-domain bases* (SDB) are instead employed. These are expansions defined over smaller *patches* or *segments*, $\Delta G_i(\mathbf{r})$, of the object, and can be written as

$$f(s') = \sum_{i=1}^{X_S} \sum_{j=1}^{N_i} I_{ij} U_i(s') b_{ij}(s') \text{ with } U_i(s') = \begin{cases} 1 \text{ for } s' \in \Delta G_i(\mathbf{r}) \\ 0 \text{ otherwise} \end{cases} \qquad (11a)$$

where the number of subdomains is X_S and the basis $b_{ij}(s')$ has N_i terms on segment i, an example of which is the three-term basis

$$I_i(s) = A_i + B_i \sin[k(s-s_i)] + C_i \cos[k(s-s_i)];\ \text{where } |s - s_i| \le \Delta_i/2 \qquad (11b)$$

Normally, this kind of multi-term basis is the same for all subdomains, except for boundaries such as the ends of wires or edges of strips. Two or more terms in each subdomain basis may be employed to produce some specified degree of continuity in the unknown at segment junctions, which also reduces the total number of unknowns in (11) from $X_S N_i$ to of order X_S. Hybrid combinations of EDB and SDB have also been found to be useful [12].

3.3.2 *Sampling* the defining equations and forming a *linear system of equations*

--This step can be expressed, for the case of the EDB, as

$$\int_{G(\mathbf{r})} t_j(s), L(s,s') b_i(s') ds = \int_{G(\mathbf{r})} t_j(s), g(s) ds,\ j = 1, \ldots, X_S, \ldots, N_T \qquad (12)$$

where $t_j(s)$ is the j'th testing function. There are normally at least X_S testing functions

so that (12) generates as many equations as unknowns. A similar equation also holds for the SDB. As for the basis functions, the testing functions can be either entire-domain or sub-domain, or some combination thereof. One of the more commonly used subdomain testing functions is the delta function, in which case the integral (12) samples the fields at a set of N_T discrete points on the object being modeled. The use of other kinds of testing functions essentially varies the contribution of the boundary field at a given point on the object to the final matrix coefficients in proportion to the value of the testing function at that point. For mathematical reasons, it can be advantageous to employ the same functions for both the basis and testing functions, an approach that is known as Galerkin's method [11].

Each equation sample involves an operation or FLOP count that is a constant for DEs and is proportional to X_S for IEs. The DE FLOP-count dependency is lower because all of the terms in a DE are collocated in space. The DE field therefore involves only neighboring fields/sources (F/S) through sampled approximations of the differential operators, thus requiring a fixed number of terms per equation sample. The IE field, on the other hand, involves F/S over the entire surface on which tney reside through a sampled summation which has X_S terms. The total FLOP count for this step is therefore proportional to N_T for DEs and $N_T X_S$ for IEs.

This steps results in

$$\sum_{j=1}^{X_S} Z_{i,j} I_j = V_i;\ i = 1,\ldots,X_S,\ldots,N_T$$

where (13)

$$Z_{i,j} = \int_{G(\mathbf{r})} t_i(s) L(s,s') b_j(s') ds \text{ and } V_i = \int_{G(\mathbf{r})} t_i(s) g(s) ds$$

with $Z_{i,j}$ the coefficients of the system, or impedance, matrix as it is called for an IE EFIE model. We note that when $N_T > X_S$, which results in more equations than unknowns, a solution to (13) can be obtained by method of least squares, or using a pseudo inverse, which is achieved by "squaring" the overdetermined impedance matrix by multiplying it by the complex conjugate of its transpose. This approach is equivalent

to implicitly imposing $N_T - X_S$ auxiliary relationships among the testing equations. Alternatively, an explicit relationship could be employed, for example using weighted sums of the sampled equations to reduce their numbers. Using $N_T < X_S$ is also permitted, which results in more unknowns than equations, in which case the number of unknowns must be decreased. This can also be done by the use of the pseudo inverse, which as before introduces implicit auxiliary relationships among the basis functions. This is equivalent to representing the current using weighted sums of the basis functions, which can also be done explicitly as in the Numerical Electromagnetics Code (NEC) [13].

3.3.3 ***Solving*** **the linear system of equations**--A solution to (13) can be formally written as

$$I_i = \sum_{j=1}^{X_S} Y_{i,j} V_j \text{ where } [Y] = [Z]^{-1} \tag{14}$$

but an inverse is seldom actually computed, the solution more often obtained in factored form or using iterative techniques, with $Y_{i,j}$ the coefficients of the solution, or admittance, matrix as it is called for an IE EFIE. The FLOP count for this step varies from X_S to $(X_S)^3$, the former for DE models solved via iteration to the later for IE models solved using LU decomposition. As problem size and complexity increase, the solution step will eventually dominate the overall FLOP count, and is an active area of current research to reduce the operation count [14].

3.3.4 ***Time sampling*** **in a time-domain model**--This step is needed to develop the time-sampled behavior as a sequence of updated, sampled spatial responses. Time stepping can be implicit, where interactions are permitted between the various spatial samples during the updating at the most recent time step, or explicit, where these interactions do not occur. The possibility of an explicit solution is a direct consequence of causality, or the fact that light propagates at a finite speed so that a change in the source located at $\mathbf{r}'$ at time t' is not known at $\mathbf{r}$ until time $t = t' + R/c$. The implicit approach requires solution of a linear system at each time step whereas the explicit

approach does not. Instead, it produces an algebraic, i.e. non-matrix solution, which is computationally more efficient, but which limits the time-sample interval to some maximum value [15]. For example, $\delta t \leq \Delta x/c$ is required in one dimension, where Δx is the space-sample size, with similar limitations applying in two- and three-dimensional problems.

3.4 Exploiting Symmetries

Many problems in electromagnetics exhibit various kinds of symmetries such as rotation, translation and reflection. When part or all of a given problem has such symmetries, they can be extremely effective in reducing computer storage and time requirements. This arises from the fact that the MM impedance matrix then has a known structure whose effect is to reduce the number of different coefficients in the matrix. An n-sided regular polygon, for example, modeled using one segment per side then has only n, rather than n^2, different matrix coefficients, producing an impedance matrix called circulant. This matrix can be solved with an operation count of order n, rather than the n^3 that would otherwise be required. More about symmetry effects can be found in [16].

3.5 Some Observations

It is worthwhile summarizing some of the key differences concerning application of the MM to IEs and DEs in the TD and FD as follows:

1) A DE model produces a linear system that is very sparse, i.e. all but some small, fixed number of its coefficients are zero, because a DE samples the F/S *locally* whereas an IE samples *globally* over some boundary.

2) The coefficients of both the DE and IE models are complex numbers in the FD but real numbers in the TD.

3) For homogeneous-region problems, the number of *spatial* source/field and equation samples using a DE model is proportional to frequency^D, where D (= 1, 2, 3) is the problem spatial dimensionality, whereas that for an IE model is proportional to f^{D-1}. This is because the former must sample fields on some *mesh* throughout the problem volume whereas the latter needs to sample only on some enclosing *surface*.

4) For problems involving infinite exterior domains, the DE model requires some kind of *closure condition* to terminate the solution mesh, whereas the IE model has a built-in radiation condition because of the Green's function used in its formulation.

5) All FD models require solution of a linear system of equations, whereas their

TD versions can be solved without matrix solution when an *explicit* treatment is used, for which the time steps are small enough that neighboring spatial samples of the F/S do not interact within the same time step. When same-time-step interaction is allowed in a TD model, they are called *implicit* formulations.

6) TD models are solved as initial-value problems using time stepping, whether implicit or explicit, and whether DE or IE models.

7) Transient results can be obtained directly using a TD model or via transformed FD results in general, but for nonlinear, time-varying media and/or components, a TD approach would normally be the better choice.

8) A TD model can a provide wideband solution valid up to some maximum frequency, f_{max}, but for a single spatial excitation, whereas a FD model can provide a solution valid for arbitrary spatial excitation but for a single frequency.

4.0 MODEL EXTENSIONS

The preceding discussion covered the basic elements of MM modeling. We now briefly examine some topics associated with making these models more efficient or more widely applicable.

4.1 Special Green's Functions for Integral Equations

Most IEs are based on the free space Green's function, so that the only boundary condition they explicitly satisfy is the Sommerfeld radiation condition. While this results in the simplest kernel function for the integral equation, it means that the induced sources which reside over any portion of S become part of the unknowns whose solution is required. An alternative approach is to employ special Green's functions that automatically satisfy the required boundary conditions over part or all of S. While such Green's functions can significantly complicate the IE kernel, at the same time they can greatly reduce the number of unknowns in the MM model, and thereby decrease the overall computer time required.

As might be anticipated, such special Green's functions are available for only a limited number of geometries for which wave-equation solutions can be obtained by separation of variables. Even though this does limit their generality, these Green's functions can be effective for problems having components possessing these special geometries. Some examples worth mentioning here are the sphere, parallel-plate waveguides, and infinite planar surface.

Some satellites have basic spherical shapes with various additional wire appendages, panels, etc. Use of the Green's function for a point current source near a sphere means that a model for this kind of object will involve as unknowns only the currents flowing on its non-spherical parts [17]. This idea has been generalized to bodies of rotation (BOR) having wire appendages, so that a solution can be developed as a series of modes varying as $I_n(s)e^{jn\varphi}$ [18], [19], [20]. A BOR exhibits one of the kinds of symmetry that can be exploited to increase solution efficiency, as already mentioned above. We note that rotation symmetry arises in both continuous and discrete forms, the former being exhibited by a circular loop and that latter by an n-sided regular polygon as an

approximation thereto.

In ElectroMagnetic Pulse (EMP) studies, it is common to employ parallel-plate waveguides as simulators to measure the response of test objects to an impulsive, planewave field. A MM model of such interactions can be more efficiently evaluated using a Green's function for a current source located between parallel, infinite conducting planes [21]. This approach has also been extended to rectangular cavities for model the mode-stirred chambers being used for ElectroMagnetic Compatibility (EMC) analysis [22].

The problem of two half spaces of different electrical properties having a common, infinite, planar interface is one which well describes the environment of at least two classes of antenna problems. One is that of communications antennas operated at frequencies below 100 MHz located near the surface of the earth, for which the Sommerfeld integrals are the special Green's functions [23], [24] and which will be discussed more below. The other is the problem of microstrip geometries, which at frequencies up to 100 GHz and higher are finding increasing use as antennas, and at lower frequencies but in much smaller sizes are found in very large scale integrated circuits where field effects are being found increasingly important [25], [26], [27], [28]. More general layered-media problems have also been modeled, including anisotropic layers [29], [30], and multiple layers [31], [32], [33].

4.2 Hybrid Models

Many of the problems needing analysis today exhibit features not well suited to any single kind of model. For example, although IE models are generally best for modeling perfectly conducting, or homogeneous penetrable object, for which they require only surface sampling in contrast with DE models which require volumetric sampling, when the penetrable object is spatially *inhomogeneous*, then the IE model also requires volumetric sampling. But since the IE matrix has all nonzero coefficients (see section 3.3 below), or is *dense*, compared with the DE matrix which is always *sparse*, the DE approach would generally be the better choice for inhomogeneous objects. It follows that when a problem involves a combination of inhomogeneous and perfectly

conducting objects, using both the IE and DE approaches together in a *hybrid* model would often be more efficient than modeling the entire problem using either approach alone.

Such hybrid models are becoming more commonly employed in CEM [34]. One of the first examples employed the geometrical theory of diffraction (GTD) and the MM to handle wire antennas located near the edge of a ground plane [35]. The GTD diffraction coefficients were used to calculate the fields scattered from the edge so its effect could be included in an IE model for which the unknown current remained only that on the antenna. Other hybrid models have combined DEs and IEs [36], modal expansions and IEs [37], and low-frequency results with IEs [38], as well as extended the GTD-IE models [39], [40], [41], [42]. The basic motivation for development of such hybrid approaches is the goal of modeling each of the separate parts of a complex problem with a technique that is best suited to its particular characteristics. As the problems needing solution becomes more complex, the need for hybrid models will continue to grow.

4.3 Modeling Slots and Apertures

Perhaps the simplest class of antennas to model are those composed of wires. As demonstrated by the collection of articles in this special issue however, wires represent a relatively small set of antenna geometries of interest, even at low frequencies. Other geometries include microstrip structures and aperture antennas, both of which generate the need to handle more general body shape having narrow slots and apertures. Many of these problems effectively result in the entire body in which the slot or aperture is placed acting as the antenna with its excitation being provided by apertures or slots in its surfaces. Models based on the numerical techniques being discussed here can be developed for such problems [43].

Slot antennas are usually defined to be narrow, extended apertures which, when located in an infinite, plane conducting sheet are described by a Pocklington-type IE [44]. The unknown in this case is the voltage across the narrow dimension of the slot as compared with the longitudinal current on a thin wire. Slots and antennas composed of thin strips of metal are called dual structures [45], so named because their mathematical

descriptions are identical with a suitable interchange of variables. But more general apertures are not solvable using duality, and their modeling requires careful consideration of the fields in the aperture as well as over the surface in which it is located. The problem of modeling apertures and slots is closely related to the so-called source problem, that of defining circuit quantities for antennas for which thin gaps or slots are most often used for their excitation, which is discussed briefly below in Section 6.1.

4.5 Modeling Imperfectly-Conducting Objects

Our discussion thusfar has addressed primarily the problem of modeling perfectly conducting objects. Because high antenna efficiency, i.e., the ratio of radiated to input power, is usually desirable, most antennas are made so as to minimize dissipative loss. This is in contrast to the fabrication of "low-observable" targets where the goal is to absorb energy from the incident field to minimize the scattered radiation. Thus, "perfect-conductor" antenna models are applicable to a large proportion of low-frequency antenna applications.

Never-the-less, it is desirable that these models also include a capability for handling imperfectly-conducting objects. Applications for this capability include use of reactive loading to decrease the physical size at which a structure is resonant and for impedance matching, and where the antenna's environment includes dielectric or lossy materials as is increasingly the case with the use of composites and other specialized materials. The analytical and numerical rigor needed for modeling imperfect conductivity depends on problem requirements and characteristics. For wires, two kinds of extensions to perfect conductivity have been employed. One is the use of impedance loading on the wire to account for the effects of lumped loads, such as might represent the generator impedance, or distributed loads as a means of modeling finite conductivity, or to handle transmission-line interconnection (TLI) between two ports on the antenna [13]. The other is to approximate the effects of dielectric sheaths which are frequently used for buried antennas by radially-directed displacement currents [46].

The effect of an impedance load can be accommodated in (13) simply by including a

voltage drop on the RHS to obtain

$$\sum_{j=1}^{X_S} Z_{i,j} I_j = V_i - I_i Z_{iL};\ i = 1,\ldots,X_S,\ldots,N_T \qquad (13')$$

where Z_{iL} is the load on segment i. Note that unless TLI loading is employed, the load terms affect only the diagonal entries of a modified impedance matrix. For surfaces, an equivalent procedure is to employ a surface-impedance term, which relates the electric and magnetic surface-currents **J** and **K** as $\mathbf{K} = Z_S \mathbf{n} \times \mathbf{J}$, where Z_S is the surface impedance. In this case, there are no additional unknowns beyond those required for a perfect conductor. More generally, both **J** and **K** need to be found from an IE derived from imposing continuity of both **E** and **H** across the surface, a topic not pursued further here.

5.0 COMPUTATIONAL ISSUES

We discuss here a number of issues that must be considered in selecting a model or computer code for application to a given problem or class of problems. We begin by first briefly examining the desirable *attributes* of a useful computer model, followed by a more detailed discussion of how these attributes are affected by the analytical and numerical treatment on which a model is based and its intended applications.

5.1 Desirable Model Attributes

Although there are many equivalent ways in which the desirable features of a useful computer model can be described, in one way or another the most basic model attributes desired by most users would be accuracy, efficiency, and utility. We briefly discuss these issues here.

5.1.1 Accuracy/Reliability--The quantitative degree to which the computed results conform to the mathematical and physical reality being modeled. It is determined by the physical modeling error (ε_P) and the numerical modeling error (ε_N).

5.1.2 Efficiency/Productivity--Following accuracy as a desirable attribute is efficiency, the relative cost of obtaining the needed results. It is determined by the human effort required to develop the computer input and interpret the output, and by the associated computer cost of running the model.

5.1.3 Utility/Applicability--The applicability of the computer model in terms of problem size and complexity. Utility also relates to ease of use, reliability of results obtained, etc.

5.2 Model Accuracy/Reliability

Above all else, a modeling computation must posses acceptable, preferably known, and better yet "dialable" accuracy. This is an attribute to which all others, however desirable they might be, must be considered secondary, for invalid results have no value and can even be detrimental. Of the two basic modeling errors, ε_P comes from replacing the real physical problem with an idealized mathematical representation, while

ε_N come from obtaining an approximate numerical solution for that idealized representation.

For only a few problems is ε_P possibly zero, a sphere for example The physical-modeling error can arise in several different ways, including using a simplified or different shape for the numerical model, such as approximating a circular loop by a polygon. Other causes of ε_P are using a different kind of object, such as a wire mesh in place of a solid, continuous surface, or even different material constants. Their actual values may be not be available to the needed accuracy, or they may be approximated, one example being use of a perfectly conducting ground plane in place of a lossy, penetrable ground. In most cases, ε_P will be the largest error source and ultimately requires experimental measurement for its assessment.

On the other hand, ε_N can usually be made acceptably small in principle, but possibly at the expense of increasing X_S beyond a computationally affordable limit, since for large X_S it varies approximately as $\exp(-kX_S)$ [47]. This is because the difference that can exist between the computed result and an exact solution, the solution error, is caused by using a finite number of unknowns. Also contributing to ε_N is the equation error, which results because of roundoff due to using finite-precision computations, however many unknowns are used. Another source of ε_N includes omitting details of the mathematical representation in the numerical model. In wire modeling, for example, although the actual currents flowing near wire junctions can be expected to exhibit azimuthal variation, this effect is normally not included in the numerical model, as is also the case of the endcap currents flowing on the ends of wires.

Although experimental data remains the preferred way to validate numerical results, most model developers and users rely heavily on "convergence" tests to determine whether the numerical results are converging towards some limiting value as X_S is increased. Convergence tests should be regarded as a necessary, but not sufficient,

condition for a model to satisfy, since convergence to the correct result is not guaranteed. Furthermore, the appearance of convergence can depend on what computed quantity is being examined. A simple example is presented in Fig. 1, where the input impedance and admittance of a two-wavelength long, center-excited dipole antenna is plotted as a function of the number of unknowns, as obtained using NEC [13]. These two kinds of results, both obtained from *the same model*, being related as $Z = 1/Y$, could lead to quite different conclusions about the validity of this simple model for a given number of unknowns. Although the admittance results exhibit acceptable convergence, the impedance data seems to imply that many more unknowns are required to achieve the same degree of convergence. This shows that care must be used in interpreting convergence tests, especially when complex numbers are involved where resonance effects can arise.

Generally speaking, most low-frequency EM models require a sampling density equivalent to six to twenty samples per wavelength to obtain acceptable results, for which the normalized convergence error can then be expected to be in the range of 0.01 or less. There are actually two kinds of effects that drive the required sampling density. For smooth, extended geometries such as a sphere as the idealized example, the sampling density is truly "wavelength" driven, with X_S determined primarily by overall electrical size. When the object is more geometrically or electrically complex, the required sampling density can become much greater in order to resolve the rapid changes in the F/S that can occur near discontinuities or rapid changes. This point is made is Fig. 2 where the convergence in the tumble-average, backscattered fields for a number of wire objects is presented as a function of sampling density [47].

Application-relevant, model-independent validation measures are needed for quantitatively assessing the accuracy of computed results. Some of the categories of results that might be useful include: 1) far-field quantities [radiation/scattering pattern, total radiated power]; 2) near-field quantities [local electric and magnetic fields, reactive and real power flow]; 3) boundary quantities [total tangential electric field on perfect conductor]: 4) approximation effects [the effects for bends and wire ends normally ignored in wire models].

An example of a boundary-condition check is included in Fig. 3 where the magnitude of the tangential electric field produced by the current excited on a center-fed dipole modeling using a point-matched solution to the EFIE with a three-term current basis is plotted. This field should be zero except in the source region where it should negate the applied excitation, but as can be observed here, it is zero numerically zero only at the match points. This result, which is rather typical, shows that the required boundary conditions may be satisfied only approximately by a numerical solution. A more appropriate quantitative measure of how well the boundary conditions are satisfied is provided by an integral of the boundary-field error divided by the incident field, which for this case would be near 0.01, comparable to the result that might be expected from a convergence test.

5.3 Model Efficiency/Productivity

While it is obvious that a model that efficiently produces inaccurate results has no value, it is equally true that a model that produces acceptably accurate results but which requires computer and/or human resources incommensurate with the application has little more value. As mentioned above, from the viewpoint of the overall cost of achieving a specified accuracy for the electromagnetic observables needed from a given model, efficiency involves two components: computer and human. The computer cost itself might be stated in several ways including total CPU time or the money charges of the computation. A more relevant and hardware-independent measure of the computing cost would instead be provided by estimating the total number of FLOPS required for the overall computation. It might be even more informative to multiply this number in turn by the number of bits manipulated per FLOP to establish the total number of bit operations, or BLOPS, required for the model computation to be accomplished to some acceptable accuracy.

The BLOP count could be especially significant in comparing two otherwise similar models applied to the same problem when one of them requires higher-precision computations because it is less well conditioned. The FLOP count, on the other hand, could be more relevant when one of the models produces unused information relative to

the other. An example of the latter situation is that of computing the factored form of the impedance matrix when using an IE model for an antenna problem where a solution is needed for only one excitation, in which case an iterative procedure can be more efficient for one or a few RHSs.

Although all electromagnetic models proceed from Maxwell's equations, their particular formulation or numerical implementation may result in substantial differences in the kind and amount of information provided by the basic computation. A DE-based model, for example, provides the spatial fields throughout some solution volume whereas an IE-based model normally yields only the sources over bounding surfaces. Matrix solution by factorization provides a RHS independent solution matrix whereas iteration requires that an entirely new solution be computed for each new RHS. It might be useful to define a measure of *information efficiency* for given models applied to given problems. One possibility would be that of dividing the information concerning electromagnetic observables actually needed in the application by the total information given by routine use of the model. For antenna problems which involve a single point of excitation but which are modeled using an IE-based code which solves the impedance matrix by factorization, this efficiency measure would be of order $1/X_S$ since only the equivalent of X_S.

One aspect of efficiency that is not so dependent on the formulation, numerical implementation, and solution procedures as it is on the user interface provided by a model's developers is the *user efficiency*. Thus, a model which that be deficient with respect to user efficiency but which is otherwise attractive could be improved with the addition of more "user-friendly" interfaces. For a user choosing among competing models and having less demanding applications, user efficiency could be the most important overall factor in making a selection.

Each of the above measures of efficiency might be combined in an appropriately weighted sum to derive some *overall efficiency* measure, the weights being determined by the importance of each component to a prospective user of a given code.

5.4 Model Utility/Applicability

Finally, we must consider a model's utility in terms of the kinds of problems to which it can be applied. At this stage, general-purpose modeling codes and specialized, single-problem codes become most differentiated. On the one hand, it is always easier to develop a model specialized for a particular problem that will be more accurate and/or efficient than a general-purpose code that can model that same problem. On the other hand, the more widely applicable a given modeling code becomes, and the more easily used it is, the greater its utility for the non-specialist who does only infrequent modeling.

This attribute is perhaps less easily defined than accuracy or efficiency but can be regarded as including all those factors not included in either. Utility essentially measures the kinds of problems for which a model might reasonably be used. Among the factors which comprise utility are: 1) geometrical configurations permitted; 2) electrical characteristics included [perfectly conducting, impedance-loaded, homogeneous penetrable, inhomogeneous, anisotropic, etc.]; 3) kinds of excitations [plane wave, dipole sources, Gaussian beams, local voltages]; 4) solution domain, FD or TD; 5) input/output requirements needed to express real-world problem in model terms; 6) hardware requirements [what computers,what interface hardware, word-size requirements, storage needed, etc.].

5.4 A Comparison of Model FLOP Counts

As discussed above, the spatial sampling required of any of the models considered here is driven by the wave-nature of electromagnetic fields, involving X_S total spatial unknowns. For resonance-region modeling, where a characteristic dimension, L, of the object to be modeled is in the range $0.1 \leq L/\lambda \leq 10$, the minimum equivalent sample density is on the order of 5 to 10 spatial samples per wavelength, but can be much greater for geometrically complex objects. A comparison of convergence rates for several different methods used to model scattering from a straight wire about 12 wavelengths long is shown in Fig. 4.

Besides the spatial-sampling required whether using an FD or TD model, there is also

the additional temporal sampling required of TD modeling, which is on the order of 5 to 10 temporal samples per period of the highest-frequency component in the response. Furthermore, we note that TD models are required to be "run" or time stepped over some minimum time duration of order L/c to achieve a steady-state response when time-harmonic excitation is used, or to obtain a converged result when the excitation is wideband. This minimum time is needed to allow the farthest extremities of the object to interact, and involves a total number of time samples X_T.

The number of samples needed to model a problem is the principle parameter determining the computer time required for its solution, since we should expect the overall FLOP count to grow at least as fast as X_S for FD models and $X_S X_T$ for TD models. But because the amount of computation required per sample can itself be a function of the number of unknowns, the actual FLOP count can grow much more rapidly than this. For example, a FDIE, while involving X_S unknowns can require on the order of $(X_S)^2$ FLOPs per unknown to compute an inverse or factor the impedance matrix, since the total number of operations varies as $(X_S)^3$. Summarized in Table I are the frequency dependencies of some of the more commonly used FD models. In this table, D is the problem dimensionality (D = 1 for plane-layered media, D = 2 for infinite-cylindrical geometries and wires, and D = 3 for general, three-dimensional problems. Also, N is the operation count per unknown, S is the number of additional operations per RHS, and H is the total number of RHSs needing solution.

TABLE I--Frequency Dependence of X_S, N, and S for IE and DE Frequency-Domain Models

	IE Homogeneous	IE Inhomogeneous	DE
Sample Count X_S	f^{D-1}	f^D	f^D
Operation Count per Unknown N			
Iteration	f^{D-1}	f^D	*Constant*
LU Decomposition	$f^{2(D-1)}$	f^{2D}	$f^{2(D-1)}$
Total Operations for Single Solution			
Iteration	$f^{2(D-1)}$	f^{2D}	f^D
LU Decomposition	$f^{3(D-1)}$	f^{3D}	f^{3D-2}
Operations per Additional RHS S			
Iteration	$f^{2(D-1)}$	f^{2D}	f^D
LU Decomposition	$f^{2(D-1)}$	f^{2D}	f^{2D}
Total Operations for H RHSs, or *Complexity*			

Iteration	$Hf^{2}(D-1)$	$Hf^{2}D$	HfD
LU Decomposition	$f^{3}(D-1)$ + $Hf^{2}(D-1)$	$f^{3}D$ + $Hf^{2}D$	$f^{3}D-2$ + $Hf^{2}D$

6.0 REPRESENTATIVE APPLICATIONS/CAPABILITIES

Space limitations permit but an brief overview of what present low-frequency antenna modeling capabilities and applications include. Considering the necessity of covering at least the basic ingredients of the analytical formulation and details of the numerical implementation and computational issues, we can include here only a sparse sampling of applications. We first discuss one of the most important aspects of low-frequency antenna modeling, that of modeling the source used to numerically excite the antenna. We then present FD examples for infinite-media applications, environmental effects such as the earth-air interface and mounting structures for antennas, and special modeling issues. The section is concluded by brief consideration of TD applications.

The relative importance of the various physical characteristics that might be used to describe low-frequency antenna performance, such as input impedance, current distributions, the near fields, the radiation pattern, radiation efficiency, etc. depends on the needs of a particular application. In most applications, the frequency dependance of the input impedance would be of most concern because of the need to design matching circuits. This would be closely followed by the radiation efficiency, with the importance of the radiation pattern be somewhat more variable, depending on the use intended for the antenna. For some communication's applications, it may be necessary to produce a pattern that is isotropic to some prescribed degree in a particular plane, while for direction finding, the location and depth of nulls is critical. The examples presented here illustrate some of these aspects, starting with the fundamental problem of source modeling.

6.1 Source Modeling

Antenna input admittance is defined as the current per unit voltage at the excitation port. Although a circuit quantity, it must be derived from antenna fields, since while the current at a given point on the antenna can be uniquely defined, the voltage is an integral quantity whose rigorous evaluation would require integration of the field across the source region. For point-sampled thin-wire models, where the field is fixed only at discrete points, the variation of the electric field between match points is not known, so finding the effective drive voltage would require evaluation

and integration of the electric field after the current distribution has been computed. This process can require as many, or more, FLOPs than filling the impedance matrix. One way to avoid this problem is to assume that the incident or exciting electric field, E_{ex}, is constant over the segment to which the excitation is applied, and zero elsewhere, so that the voltage can be approximated as $V_{ex} \sim -E_{ex}\Delta$ where Δ is the length of the source segment, which is sometimes called the "gap" model [13]. The plot in Fig. 5 demonstrates the potential difficulty of defining the exciting voltage from a single sample of the tangential electric field [48]. A magnetic field, "frill-source" model has also been employed [49], which seems best suited for "thicker" wires.

This model, and even more numerically robust ones where the tangential fields are integrated by using testing functions that sample the fields along the wire, are reasonably reliable. However, they do not include the capacitance of feed wires or structure that are normally required to connect the antenna to a physical generator. Some results are shown in Fig. 6 to demonstrate this effect. Two results for the frequency dependence of a dipole antenna input admittance are presented, one for the point-sampled simple source model just described and the other which uses a transmission line (TL) to excite the dipole, also modeled using NEC. A downward shift in the resonance peaks can be observed in the TL model, evidently caused by the capacitive effect of the dipole-TL connection. The problem of Some other work on source models is described elsewhere [50], [51], [52], [53], [54].

6.2 Infinite-Media Applications

Many antennas are located near the perturbing effects of the ground, or structures such as vehicles, aircraft, ships, building, etc. which affect their performance. These effects are important to understand both qualitatively and quantitatively. One way of doing this is to assess its characteristics when the antenna is located in an infinite medium for comparison with these same characteristics when located in its actual operational environment [55]. For this and other reasons, much modeling deals with the simpler application of a given antenna operated in free space, or some other infinite medium.

The variety of antenna types modeled in infinite media is vast, including linear, vee [56] and folded dipoles [57] and loops [58], conical and helical [59] spirals, linear [60] and log-periodic arrays (LPA), dielectric rods [61], and others [62], [63]. The MM results obtained for such antennas are usually found to agree with measured results for input impedance and radiation pattern to high accuracy, usually within the experimental error, when the numerical model includes the important features of the measured structure. Three representative examples are shown here in Figures 6, 7, and 8. Fig. 7 displays the radiation pattern of a fore-shortened LPA [55], in which the lengths of the longer antenna elements have been reduced to a fixed value by employing lumped inductance loading to reduce their resonant lengths, as a way to make the overall antenna structure smaller. The current distribution on a conical spiral antenna as obtained using the Pocklington EFIE and the Hallen IE [64] is shown in Fig. 8, where good agreement may be observed.

An example of modeling an antenna in an infinite, plasma medium, is included in Fig. 8 [55]. This particular problem was chosen because of the desire to extend the basic NEC model to handling antennas buried in a lossy ground. In order to do this, a capability is needed of modeling antennas in infinite media having the same electrical properties. Although a somewhat specialized medium, a plasma was chosen to validate the lossy-medium extension because other results were readily available. Excellent agreement is exhibited between the TWA IE results and the quasistatic formulation described in [65].

6.3 Environmental Effects

Environmental effects on antenna performance are taken here to include any perturbation to the infinite-media behavior of the generic antenna due to changes in its near-field environment, such as represented by the earth-air interface, structures on which the antenna is mounted, or other changes in its basic structure. Examples of each area are briefly discussed below.

6.3.1 Modeling sheaths--Insulating sheaths are sometimes included on wire antennas to protect the metal from the environment or to modify the electrical

characteristics of the antenna. Ice accumulation on wires may also create a sheath. Antenna wires buried in the ground are often insulated, since a dielectric sheath can greatly reduce power dissipation near the wire. The effect of a thin sheath on the antenna characteristics can be included in the thin-wire model with relatively little difficulty using a treatment first reported by Richmond and Newman [66]. Sheath models have been included in wire antenna codes by Popovi'c et al. [67], who also allows ferrite coatings, and in a version of NEC [68] which includes interface effects.

To model the effect of a sheath, the field due to radial polarization currents in the sheath is included in enforcing the boundary condition on the wire. For a wire with radius a and sheath radius b, the insulating sheath with complex relative permittivity $\varepsilon_{r2} = \varepsilon_2 - j\sigma_2/\omega\varepsilon_o$ in a medium with $\varepsilon_{r1} = \varepsilon_1 - j\sigma_1/\omega\varepsilon_o$ is replaced by an equivalent polarization
current of

$$\mathbf{J}_s(\rho,z,\varphi) \approx j\omega\varepsilon_o(\varepsilon_{r2} - \varepsilon_{r1})[\mathbf{E}^s(\rho,z,\varphi) + \mathbf{E}^{inc}(\rho,z,\varphi)]$$

$$\approx -(\varepsilon_2 - \varepsilon_1)I'(z)\rho/(2\pi\,\varepsilon_{r2}\rho); \qquad a \le \rho \le b$$

radiating in medium 1. $\mathbf{E}^s$ is the electric field due both to currents on the wire and to $\mathbf{J}$ itself, and $\mathbf{E}^{inc}$ is the excitation field. To retain a one dimensional integral equation for the axial wire current, the sheath is assumed to be electrically thin, and the total field in the sheath is assumed to be dominated by the radial field due to charge on the wire. The field due to $\mathbf{J}_s$ is needed on the wire axis, which for a straight segment of insulated wire with $|k_1 b| \ll 1$ can be approximated in terms of the second derivative of the axial current as $j(\varepsilon_2 - \varepsilon_1)I''(z)\ln(b/a)/[2\pi\,\omega\varepsilon_o\varepsilon_{r1}\varepsilon_{r2}]$ [68], which is included in the total, axial electric field in the thin-wire integral equation.

The accuracy of the thin-wire sheath model for insulated wires in air has been demonstrated by comparison with measurements in [24] and [67]. An comparison of results obtained using this sheath model with independent data is included in Fig. 10. A totally different approach for modeling sheaths using a Wiener-Hopf approach [69] is presented in Fig. 11.

6.3.2 Modeling the earth-air interface--At frequencies below VHF, many antennas necessarily include the earth-air interface as part of their near-field environment. An analytically rigorous formulation for such problems begins with the Sommerfeld-integral fields, or their equivalents [23], by which the fields of vertical and horizontal point-current sources near an interface are represented as infinite-domain, Fourier-type integrals. In an IE model, these integrals form part of the IE kernel, and can increase the FLOP count associated with the MM impedance matrix evaluation by a factor of 100 or even more. Using model-based parameter estimation (see Section 6.4 below) to replace the Sommerfeld fields with more computationally efficient approximations can reduce the FLOP to near that of the infinite-medium problem. Use of this approach to model a vertical, base-fed monopole antenna connected to one to three wires parallel to the ground to act as a sparse, directive ground screen is illustrated in Fig. 12.

6.3.4 Modeling antenna groundstakes--A more difficult problem to model is that of objects interacting across the earth-air interface, since then the fields on both sides of the interface are required. The approach described above can be extended to this kind of problem, but requires accounting for the fields reflected from, and transmitted across, the interface. This makes possible modeling the behavior of monopoles excited against a ground stake, the combination of which is represented as a single wire that is vertical to, and penetrates, the interface. A result for this kind of model is shown in Fig. 13 [23], where the input resistance and reactance are presented. Since the radiated power can be obtained by integrating the far-field in air, this model makes it feasible as well to compute the antenna efficiency where power absorbed into the ground is the loss term.

6.3.4 Modeling ground screens--Most ground screens consist of many more radials, and for practical reasons are buried rather than elevated. The approach just described can be effective for this kind of problem as well, for which a sample result is presented in Fig. 14, where the difference in input impedance of a monopole driven against a perfect ground and against a buried ground screen having N evenly-spaced wires is shown as a function of the screen radius. The plotted points are

obtained from a compensation approach [70] and the continuous curves from the NEC model [8]. Good agreement is obtained in the region where the approximation is valid, providing mutual validation of these independent results and demonstrating the utility of the Sommerfeld-based formulation.

6.3.5 Modeling ground probing--Antennas located in free space above the ground can be used to detect subsurface anomalies, a principle exploited in metal and mine detectors. A sample result is shown in Fig. 15 for this kind of application, again based on the NEC model [8],[13]. Detectability of subsurface features can be based on impedance variations of a scanning antenna or on measurements of the total field near the interface due to some independent source field and that scattered from a subsurface target.

6.3.6 Modeling sheathed wires near the earth-air interface--When an insulated wire is embedded in a medium such as earth or water the current tends to have a sinusoidal form, as for a bare wire, but the wave number may be orders of magnitude less than for a bare wire in the medium. Use in (11b) of a wavenumber equal to the wave number in the surrounding medium can then result in slow convergence of the solution [70]. A more appropriate value for k_s can be obtained from an approximation for the wave number on a buried insulated wire developed from the theory of coaxial transmission lines [71], given by $k_L \approx (1 + H_0^{(2)}/[k_1 b \ln(b/a) H_0^{(1)}])$ where k_1 is the wave number in the infinite medium, k_2 is the wave number in the insulating material and $H_0^{(1)}$ and $H_0^{(2)}$ are Hankel functions of order 0 and 1 and argument $k_1 b$.

Results of the NEC model for buried insulated wires have been validated by comparison with an independent boundary-value solution developed by Wait [72] for an insulated wire in a lossy medium including an interface. The propagation constant $\Gamma = \alpha_L + j\beta_L$ was determined from the NEC solution by fitting a function $I_0 \exp(-\Gamma x)$ to the numerically determined current. Results of a NEC model for a buried insulated wire including an interface are compared with Wait's solution in Fig. 16 for varying

distance from the interface. Results for β_L are seen to be in very good agreement, while α_L shows some difference for small d, but generally good agreement overall, with a maximum error of about 5 percent.

6.3.7 Antenna-structure effects--Antennas are often mounted on complex structures, the effect of which can greatly modify the antenna's impedance, current distribution and radiation pattern. Some results are included here to demonstrate some applications to this problem. The input admittance of a monopole antenna mounted at the edge of a conducting box is shown as a function of frequency in Fig. 17 [73]. The numerical results, obtained from a surface EFIE, exhibit good agreement with the experimental measurement. A wire-mesh model of an aircraft with two wire antennas attached between the vertical stabilizer and the forward fuselage is shown in Fig. 18 [74], together with a comparison of a measured results, which again show good agreement. In this case, a shunt capacitance was added at the base of the antenna as an impedance load to the wire-grid model which itself did not adequately account for the its effect.

Large reflector antennas, especially those used on satellites, are fabricated from meshes to conserve weight and for more compact stowage. The effects of the mesh on the reflecting properties of these antennas are needed to achieve the intended gain, and so some basic studies of meshes have been undertaken using MM models. The basic idea is to define a unit cell of an infinite planar mesh and to exploit Floquet's theorem to reduce the problem to that of modeling this single cell and its interaction with the infinite array of cells [75]. Of interest in this application are the effects of finite wire conductivity and imperfect junctions at the connection points of wires in the mesh, for which some results are shown in Fig. 19.

6.4 Some Other Modeling Issues

6.4.1 Modeling endcaps--In practice there appears to be little difference between a cylindrical antenna with open ends or flat end caps [76]. However, since the validity of some implementations of the TWA requires a closed surface, it is sometimes necessary to close the wire ends to obtain a stable solution with

the thin-wire kernel. The simplest way of closing the wire end is with a flat cap. A simple first-order correction for a flat end cap has been found to yield a significant improvement in the stability of the solution with minimal increase in solution time [8]. In this treatment the singularity of charge at the edge is neglected, and a constant surface charge density is assumed on the cap, with current and charge continuous from the wire to the cap. The current density on the end cap, $\mathbf{J}_c(\rho)$ to maintain continuity with the net wire current $I_w(z)$ at the end $z = 0$, is then $\mathbf{J}_c(\rho) = \rho S I_w(0)\rho/(2\pi a^2)$ where ρ is the radial coordinate from the wire axis, a is the wire radius and S is 1 if the reference direction for I_w is toward the end cap and - 1 otherwise. The charge density on the end cap is then given by $\rho_c = j\nabla\cdot\mathbf{J}_c(\rho)/\omega = jSI_w(0)/(\omega\pi a^2)$. Also requiring continuity of charge density from the wire to the end cap yields the condition $[I'_w(z)/I_w(z)]_{z=0} = 2S/a$ which is enforced at the end of the wire in defining the three-term current basis (11b).

The effect of including caps on wire ends and voltage sources is shown in Fig. 20 for a quarter-wave monopole with a wire radius of 0.01 λ. The monopole was divided into 80 segments, so that Δ/a was 0.3125. The invalid condition of zero field on the axis of an open cylinder results in oscillations of the current at the wire end and voltage source. These oscillations become apparent for segment lengths less than about the wire diameter, although the effect of end caps may become significant before this point. Adding caps to the wire end and source, using the simple model with constant charge density, is seen to greatly reduce the oscillations in the solution.

6.4.2 Junctions of multiple and stepped-radius wires--In complex wire models it is generally advantageous to impose conditions on the current and, if possible, the charge on wires at a junction. The appropriate conditions will be exhibited by a numerically accurate solution of an integral equation, such as (4). However, accurate results will be obtained using a smaller value for X_S if physically correct conditions are imposed in the current expansion. These conditions may be introduced in equations appended to the full MM impedance matrix, but more often

they are built into the basis functions so that they are automatically satisfied in the solution for current.

The first condition, used in nearly all wire codes, is continuity of current, or Kirchhoff's current law at multiple-wire junctions. In simpler current expansions, such as a piecewise linear or pulse basis, Kirchhoff's law may be satisfied at a junction of m wires by wrapping continuous basis functions across the junction from wire i to wire $i + 1$, skipping $i = m$. Alternately, the basis function on each segment may branch onto each of the other segments with amplitudes satisfying Kirchhoff's law.

With three-term current expansions, a condition on charge, or equivalently the derivative of current, is needed to define the basis function, since there is one more degree of freedom. Determining a correct condition on charge is not as easy as for current, since the charge must distribute so that tangential electric field is minimized over the junction or, in the quasistatic form, the scalar potential is continuous across the junction. One approach is to solve an auxiliary IE at each wire junction whose purpose is to minimize the integrated electric field along the junction wires, a procedure that also avoids increasing X_S were these extra conditions to become part of the MM impedance matrix.. A condition on charge density that takes into account the proximity of a step in radius and interaction of wires at a junction has been obtained by executing a separate MM solution for each junction [8]. Any junction at which the charge cannot be determined as uniform due to symmetry is considered isolated from the rest of the structure with the wires extended to infinity away from the junction. An integral equation based on continuity of scalar potential can then be written for the junction of m wires as

$$\sum_{n=1}^{m}\int_0^{\infty} q_n(s')\frac{e^{-jkR_{in}(s,s')}}{R_{in}(s,s')}ds' = C;\ i = 1,\ldots,m;\ 0 < s < s_{max}$$

$$\sum\int q_n(s')\{\exp[-jkR_{in}(s,s')]/R_{in}(s,s')\}ds' = C:\ i,n = 1, \ldots, m;\ 0 < s < s_{max}$$

where $q_n(s')$ is the charge density at s' on wire n and $R_{in}(s,s')$ is the distance between the points at s on wire i and s' on wire n, and C is an arbitrary constant. The distance

s_{max} should approach zero for continuity of potential, but a finite but electrically small value is used for the numerical solution.

This charge treatment has given stable results for stepped-radius wires over a wide range of segment lengths, and also yields accurate solutions for multi-wire junctions including a fan of 18 wires in an angle of 26 degrees. The fan, forming a strip line over a ground plane, could not be modeled accurately with the equal charge densities implied by (x3). The minimum angle at which wires can meet is set by the limitation of the thin-wire approximation which typically fails as the match point on one segment approaches within about a wire radius of the surface of the adjacent wire.

6.4.3 Wires at interfaces and surfaces--Several other conditions may occur at a wire end that call for alternate junction treatments. When a wire is connected to a perfectly conducting surface the charge, or derivative of current, is set to zero at that end. If the wire meets the surface at an angle from normal the charge will vary around the wire circumference. However, since the current and its image must form an even function about the plane, zero charge is the appropriate condition in the thin-wire approximation. In addition, if the wire connects to a surface on which the current is computed with a surface MM solution, a singular component is usually included in the surface current to ensure continuity of current from the wire to the surface. The typical surface current is $I(0)\rho/2\pi\rho^2$, where I(0) is the current at the end of the wire and ρ is the radial vector from the connection point.

When a wire crosses an interface between two different media the current remains continuous and charge density is discontinuous as $q_+/q_- = \varepsilon_+/\varepsilon_-$, where ε_+ and ε_- are the permittivities of the upper and lower media, respectively [77]. This condition results from the requirement of continuity of radial electric field when the penetrating wire is normal to the interface. However, the condition has been used for wires tilted by more than 60 degrees from the normal with apparently good results, based on small values of tangential electric field computed along the wire at the interface. For a lossy medium the condition on derivative of current is $I'_+/I'_- = \varepsilon_{r+}/\varepsilon_{r-}$ where ε_{r+} and ε_{r-}

are the complex relative permittivities.

No simple condition has been derived for charge at a junction of a wire with a dielectric or conducting sheath and a bare wire. In such a case, the best approach may be to include an equation minimizing tangential electric field at the junction as part of the MM equations. The same appears true when interaction with an interface has a substantial effect on charge distribution at a junction. Well-converged results have been obtained using the above derivative condition on a monopole connected to a buried radial-wire ground screen. While the derivative condition does not include the interaction of horizontal screen wires with the interface, it represents the dominant effect on charge when crossing the interface.

6.4.4 Model-based parameter estimation (MBPE)--The two most FLOP-intensive operations when doing FDIE modeling are the matrix fill and solution steps, with the one that dominates the overall FLOP count being determined by how large is X_S. For FDDE models and for explicit TD models using DEs or IEs, the solution time drives the FLOP count. Clearly, whatever part of the modeling process dominates the FLOP count, in order to improve model utility the total FLOP count needed to acquire the desired information should be minimized to the extent possible.

Limiting our attention to the FDIE, we conclude that for problems where matrix fill time is the dominant factor, which is the case of special Green's functions such as encountered for the interface problem, and where more careful integration is required by the formulation and numerical treatment, such as when using the EFIE for surfaces, it would be advantageous if computation of the interaction coefficients could be made more efficient. When the matrix solution dominates, and it is necessary to cover a band of frequencies, a commonly encountered problem, then it would be useful to either reduce the solution FLOP count and/or minimize the number of frequency samples needed over the desired bandwidth. We have mentioned that iteration is one way of reducing the solution FLOP count, from of order $(X_S)^3$ to of order $(X_S)^2$. On the other hand, for reducing matrix fill time or the number of needed frequency samples, MBPE offers an effective approach [78] , [79].

MBPE involves identifying some appropriate, preferably physically motivated, simplified representation (the *model*) which involves a small number of unknown coefficients (the *parameters*) whose numerical values are to be *estimated* in some suitable fashion. We mention two examples here of this basic idea.

As noted above, numerical evaluation of the Sommerfeld integrals that are the Green's function for the interface problem can be a FLOP-intensive operation. Using the most straightforward numerical approach, they can require up to 1,000 times the computer time otherwise needed to compute the free-space fields of the same current source. This can make modeling antennas and scatterers near the ground an impracticably expensive operation. However, it can be demonstrated that the Sommerfield fields are not that physically complex, and indeed can be well-represented by simple interpolation formulas [23]. But by using asymptotic approximations to these fields as the model, with the amplitudes being the parameters to be estimated from accurately evaluated Sommerfeld integrals, an even more efficient approach can be devised, the result of which is to reduce the matrix fill time for the problem of objects interacting across the earth-air interface to less than 10 times their free-space values. The basis for this approach is illustrated by Fig. 21. It should be obvious that the same idea can be employed in other circumstances, one example being for the parallel-plate waveguide [78].

Application of MBPE to the problem of obtaining wideband frequency results using a reduced number of frequency samples is illustrated in Fig. 22 [79]. The model in this case is a low-order rational function whose numerator and denominator orders are n and d respectively. Many fewer samples can can be used to accurately represent the frequency response in an analytical form than would otherwise be the case, for example using simple linear interpolation. Furthermore, the frequency derivatives of the response can be computed directly from a MM model for an operation count of order $(X_S)^2$, and because they provide information equivalent to another frequency sample, reduce the overall operation count even further.

6.5 Time-Domain Applications

As systems bandwidths have increased, the effects of EMP and other wideband, impulsive sources have become of concern, and wideband experimental hardware has become more available, the need to predict the transient response of antennas has attracted increasing interest. There are two basic reasons for modeling in the time domain. One is that for some particular problems, the TD models can yield the desired results more efficiently than their transformed, FD counterparts. The other is that nonlinear and time-varying media and components might be handled in a more straightforward way in the time domain.

As noted above, TD modeling involves time stepping to produce a sequence of spatial samples from which a transient response is developed. While the excitation that produces the response can be a narrowband, even monochromatic waveform, the benefit of having a TD model is not then fully exploited, which comes from using some appropriate transient excitation. One of the more useful transient excitations is exemplified by the Gaussian pulse, whose time variation is $\exp[-a^2t^2]$ and for which the frequency spectrum is $\exp[-\omega^2/a^2]$. Thus, as the coefficient "a" is made smaller, the bandwidth of the Gaussian pulse becomes broader, permitting the spectrum of the excitation to be matched to the parameters of the numerical model. A step response can be approximated by integrating the Gaussian, while derivatives of various orders might also be used [80].

The transient feedpoint receiving current for a 30-cm monopole on a groundplane, obtained from a TD EFIE and measured on a transient range are compared in Fig. 23 along with their Fourier-transformed frequency spectra. A single calculation for a TD model is seen to produce a wideband frequency response, for which a FD model would require many frequency samples to acquire equivalent information. The numerical results were computed using a TD equivalent of NEC [80], while the measured results were obtained from a TD experimental range [81]. For antenna problems like this, where a solution is needed for a single RHS, the TD model can be more efficient than performing the computation in the FD. The result of a more complex TD antenna computation is shown in Fig. 24, where a simple wire-mesh model of a truck is shown

together with the frequency variation of the bumper-mounted CB antenna. Although experimental results are not available for comparison, the VSWR of an actual vehicle having such an antenna was consistent with the predicted admittance in the CB band.

An example of using a TD model to determine the effect of a special nonlinearity is shown in Fig. 25 [80]. Here, the dipole is again excited by a Gaussian field at is center, but is loaded along its length with a series of diodes, 60 in all. The diodes are initially forward-biased by the exciting voltage, but become back-biased when the induced charge packets have flowed out to the ends of the antenna. As a result, the current in the reverse direction is much reduced, being made essentially zero, although over a long-enough time charge neutrality would once again be restored. The two pulses of far-field radiation produced by the Gaussian excitation occur initially, from the charge being set into motion at the antenna's center, and finally when the charge has stopped moving. Charge acceleration is well known as the cause of far-field radiation [80]. If the dipole were not loaded with diodes, there would be a series of radiation pulses of alternate sign and decreasing amplitude due to the succession of end reflections undergone by the charges moving back and forth along the antenna. Thus, in addition to permitting modeling of non-linearities, the TD approach also yields physical insight not as readily available in the FD.

6.6 Input/Output

As computer speed increases, making possible the solution of larger problems, the difficulty of defining the problem to be modeled and examining the results that are produced becomes commensurately greater. Computer graphics are coming to be indispensable for dealing with these input/output requirements. Two examples are included here to illustrate the value of graphics for visualizing the output. In Fig. 26 is presented one of a sequence of plots depicting the pattern of electric field motion as a function of time for a time-harmonic solution of a biconical antenna [82]. A similar kind of result is shown in Fig. 27 where the magnitude of the electric field at one instant of time produced by a Gaussian-excited conical monopole antenna obtained using a TDDE model is presented [83]. Although it is probably more obvious that such a sequence results naturally from a TD model and can be presented as in a movie, this

can also be done in the FD where time-phaser rotation creates a comparable time sequence. Visual electromagnetics is sure to become a more popular tool, of benefit to the researcher and student alike.

7.0 CONCLUDING COMMENTS

In the above discussion we have presented an overview of low-frequency antenna modeling using numerical techniques. We began by summarizing a few of the more commonly encountered equations on which these numerical models are based, limiting our specific attention to modeling perfectly-conducting objects using integral equations. A brief introduction was then given to the method of moments, a general procedure for solving differential, integral and integro-differential equations in the time and frequency domains, was presented. Some further discussion was then addressed to enhancing these basic models for more efficient or more general application, followed by consideration of some of the computational issues involved. A variety of representative applications were then presented to demonstrate some of the capabilities for low-frequency antenna modeling that are now available. A concluding point to be made here is that computational methods have joined experimentation and analysis as one of the three complementary problem-solving tools of the antenna designer. Further information and more detail about moment-method modeling can be found in a number of books and summary articles [84-91].

REFERENCES

[1] C. A. Balanis, "Antenna Theory: A Review," *IEEE Proc.*, this issue, 1991.

[2] J. A. Stratton, *Electromagnetic Theory*, McGraw-Hill Book Company, Inc., New York, 1941.

[3] W. K. H. Panofsky and M. Phillips, *Classical Electricity and Magnetism*, Addison-Wesley Publishing Company, Inc., 1955.

[4] J. Van Bladel, *Electromagnetic Fields*, McGraw-Hill Book Company, Inc., New York, 1964.

[5] A. J. Poggio and E. K. Miller, Integral equation solutions of three-dimensional scattering problems, Chapter 4 in *Computer Techniques for Electromagnetics*, R. Mittra ed., Pergamon Press, New York,1973.

[6] R. W. P. King, *The Theory of Linear Antennas*, Harvard University Press, Cambridge, MA., 1956.

[7] G. J. Burke and A. J. Poggio, *Numerical Electromagnetics Code (NEC)--Method of Moments*, Lawrence Livermore National Laboratory, Rept. UCID--18834, Jan. 1981.

[8] G. J. Burke, "Recent Advances to NEC: Applications and Validation," AGARD Lecture Series 165, 1989.

[9] A. J. Poggio and E. K. Miller, Low frequency analytical and numerical methods for antennas, in *Antenna Handbook*, Y. T. Lo and S. W. Lee, ed., Van Nostrand Reinhold, New York,1987.

[10] E. K. Miller, A. J. Poggio, and G. J. Burke, "An Integro-Differential Equation Technique for the Time-Domain Analysis of Thin-Wire Structures, I: The Numerical Method, *J. Comput. Phys.*, vol. 12, no. 1, 1973.

[11] R. F. Harrington, *Field Computation by Moment Methods*, Macmillan, New York. 1968.

[12] Medgyesi-Mitschang, L. N., and J. M. Putnam (1985), Electromagnetic scattering from extended wires and two- and three-dimensional surfaces, *IEEE Trans. Antennas and Propagat.*, **AP-33**, 1090-1100.

[13] G. J. Burke and A. J. Poggio, Numerical Electromagnetics Code (NEC)--Method of Moments Parts I, II, and III, NOSC TD 116, Naval Ocean Systems Center, San Diego. CA, (revised),1980.

[14] E. K. Miller, organizer, Special Session at 1990 AP-S Meeting, Dallas, TX, on "Reducing the operation count in computational electromagnetics, 1990.

[15] E. K. Miller, A selective survey of computational electromagnetics, *IEEE Trans. Antennas and Propagat.*, **AP-36**, 1281, 1988.

[16] E. K. Miller , "An Overview of Time-Domain Integral-Equation Models in Electromagnetics", *Journal of Electromagnetic Waves and Applications*, VNU Science Press, **1**(3), 269-293, 1987.

[17] F. M. Tesche and A. R. Neureuther, Radiation patterns for two monopoles on a perfectly conducting sphere, *IEEE Trans. Antennas and Propagat.*, **AP-18**, 692-294,1970.

[18] A. Berthon and R. P. Bills, Integral equation analysis of radiating structures of revolution, *IEEE Trans. Antennas and Propagat.*, **AP-37**, 159, 1989.

[19] R. Perez-Leal and M. F. Catedra, Input impedance of wire antennas attached on-axis to conducting bodies of revolution, *IEEE Trans. Antennas and Propagat.*, **AP-36**, 1236, 1988.

[20] H. Kawakami and G. Sato, Broadband characteristics of rotationally symmetric

antennas and thin wire constructs, *IEEE Trans. Antennas and Propagat.*, **AP-35**, 26, 1987.
[21] F. M. Tesche, On the behavior of thin-wire antennas and scatterers arbitrarily located within a parallel-plate region, *IEEE Trans. Antennas and Propagat.*, **AP-20**, 482-486,1972.
[22] Wu, D. T., and D. C. Chang, Current distribution on a thin wire in a multimode rectangular cavity, National Radio Science Meeting, University of Colorado, Boulder, CO, 1986.
[23] G. J. Burke and E. K. Miller, Modeling antennas near to and penetrating a lossy interface, *IEEE Trans. Antennas and Propagat.*, **AP-32**, 1040-1049,1984.
[24] I. V. Lindell, E. Alanen, and K. Mannersalo, Exact image method for impedance computation of antennas above the ground, *IEEE Trans. Antennas and Propagat.*, **AP-33**, 937-945,1985.
[25] P. B. Katehi and N. G. Alexopoulos, "On the modeling of electromagnetically coupled microstrip antennas--the printed strip dipole," *IEEE Trans. Antennas and Propagat.*, **AP-32**, 1179,1984.
[26] D. M. Pozar, "Microstrip antennas," *Proc. IEEE*, this issue, 1991.
[27] T. Itoh, An overview on numerical techniques for modeling miniaturized passive components, *Ann. Telecommun.*, **41**, 449-462,1986.
[28] H. Nakano, S. R. Kerner, and N. G. Alexopoulos, The moment method solution for printed wire antennas of arbitrary configuration, *IEEE Trans. Antennas and Propagat.*, **AP-36**, 1667, 1988.
[29] J. L. Tsalamengas and N. K. Uzunoglu, Radiation from a dipole in the proximity of a general anisotropic grounded layer, *IEEE Trans. Antennas and Propagat.*, **AP-33**, 165, 1985.
[30] J. L. Tsalamengas and N. K. Uzunoglu, Radiation from a dipole near a general anisotropic layer,*IEEE Trans. Antennas and Propagat.*, **AP-38**, 9, 1990.
[31] J. L. Tsalamengas, Electromagnetic fields of elementary dipole antennas embedded in stratified general gyrotropic media, *IEEE Trans. Antennas and Propagat.*, **AP-37**, 399, 1989.
[32] N. Engheta and C. Elachi, Radiation characteristics of a source in a thin substrate mounted over a dielectric medium, *IEEE Trans. Antennas and Propagat.*, **AP-36**, 322, 1988.
[33] A. Lakhtakia, V. K. Varadan and V. V. Varadan, Excitation of layered media having rough interfaces by line sources, *IEEE Trans. Antennas and Propagat.*, **AP-35**, 462, 1987.
[34] G. A. Thiele, Overview of selected hybrid methods in radiating system analysis, *Proc. IEEE*, this issue, 1991.
[35] Thiele, G. A., and T. H. Newhouse, A hybrid technique for combining moment methods with the geometrical theory of diffraction, *IEEE Trans. Antennas and Propagat.*, **AP-17**, 62-69, 1969.
[36] J. M. Jin and V. V. Liepa, A note on hybrid finite element method for solving scattering problems, *IEEE Trans. Antennas and Propagat.*, **AP-36**, 1486, 1988.
[37] A. Z. Elsherbeni and M. Hamid, Scattering by parallel conducting circular cylinders, *IEEE Trans. Antennas and Propagat.*, **AP-35**, 355, 1987.
[38] R. G. Olson and P. D. Mannikko, Validation of the hybrid quasi-static/full-wave method for capacitively loaded thin-wire antennas,*IEEE Trans. Antennas and Propagat.*,

AP-38, 516, 1990.
[39] H. T. Shamansky, A. K. Dominek and L. Peters, Jr., Electromagnetic scattering by a straight thin wire, *IEEE Trans. Antennas and Propagat.*, **AP-37**, 1019, 1989.
[40] Burnside, W. D., and P. H. Pathak (1980), A summary of hybrid solutions involving moment methods and GTD, in *Applications of the Method of Moments to Electromagnetic Fields*, B. J. Strait, ed., The SCEEE Press, St. Cloud, Florida.
[41] M. Marin and M. F. Catedra, A study of a monopole arbitrarily located on a disk using hybrid MM/GTD techniques, *IEEE Trans. Antennas and Propagat.*, **AP-35**, 287, 1987.
[42] R. Tiberio, G. Manara, and G. Pelosi, a hybrid technique for analyzing wire antennas in the presence of a plane interface, *IEEE Trans. Antennas and Propagat.*, **AP-33**, 881, 1985.
[43] R. C. Hansen, "Aperture antennas,"*Proc. IEEE*, this issue, 1991.
[44]. A. Hadidi, and M. Hamid, "A novel treatment of Pocklington's equation applied to slot antennas, *IEEE Trans. Antennas and Propagat.*, **AP-37**, 1124, 1989.
[45] R. F. Harrington,*Time Harmonic Electromagnetic Fields*, McGraw-Hill, New York, 98-100, 1961.
[46] J. H. Richmond and E. H. Newman,"Dielectric Coated Wire Antennas," *Radio Science*, Vol. 11, no. 1, 13, Jan. 1976.
[47] E. K. Miller, G. J. Burke and E. S. Selden, Accuracy-modeling guidelines for integral-equation modeling of thin-wire scattering structures, *IEEE Trans. Antennas and Propagat.*, **AP-19**, 534,1971.
[48] T. Do-Nhat and R. H. MacPhie, The static electric field distribution between two semi-infinite circular cylinders: A model for the feed gap field of a dipole antenna, *IEEE Trans. Antennas and Propagat.*, **AP-35**, 1273, 1987.
[49] Popovic, B. D., M. B. Dragovic, and A. R. Djordjevic, "*Analysis and Synthesis of Wire Antennas*", Research Studies Press, Letchworth, Nertfordshire, England, 1982.
[50] T. Do-Nhat and R. H. MacPhie, On the effect of gap width on the admittance of solid circular cylindrical dipoles, *IEEE Trans. Antennas and Propagat.*, **AP-37**, 1545, 1989.
[51] H. K. Schuman, Modeling folded dipoles and feedlines for radiation and scattering,*IEEE Trans. Antennas and Propagat.*, **AP-38**, 30, 1990.
[52] S. A. Saoudy and B. P. Sinha, Feed gap aperture field and input admittance of an infinitely long insulated antenna,*IEEE Trans. Antennas and Propagat.*, **AP-38**, 922, 1990.
[53] S. A. Saoudy and M. Hamid, Input admittance of a biconical antenna with wide feed gap, *IEEE Trans. Antennas and Propagat.*, **AP-38**, 1784, 1990.
[54] T. Do-Nhat and R. H. MacPhie, Effect of gap length on the input admittance of center fed coaxial waveguides and infinite dipoles, *IEEE Trans. Antennas and Propagat.*, **AP-35**, 1293, 1987.
[55] E. K. Miller, "Numerical modeling techniques for antennas," in *NATO AGARD Lecture Series No. 131*, Brussels, 7-1.
[56] A. J. Fenn, Element gain pattern prediction for finite arrays of V-dipole antennas over ground plane, *IEEE Trans. Antennas and Propagat.*, **AP-36**, 1629, 1988.
[57] H. A. Kalhor and A. R. Mallahzadeh, Analysis of a folded dipole antenna mounted on a cylindrical metallic mast, *IEEE Trans. Antennas and Propagat.*, **AP-34**, 99, 1986.
[58] J. W. Burns and T. B. A. Senior, The backscattered field of a thin wire loop for

H-polarization, *IEEE Trans. Antennas and Propagat.*, **AP-35**, 1049, 1987.
[59] R. G. Vaughan and J. B. Andersen, Polarization properties of the axial mode helix antenna, *IEEE Trans. Antennas and Propagat.*, **AP-33**, 10 , 1985.
[60] K. Siakavar and J. N. Sahalos, A simplification of the synthesis of parallel wire antenna arrays, *IEEE Trans. Antennas and Propagat.*, **AP-37**, 936, 1989.
[61] K. Mahdjoubi and C. Terret, An analysis of piecewise homogeneous dielectric rod antennas, *IEEE Trans. Antennas and Propagat.*, **AP-34**, 598, 1986.
[62] H. E. Green and J. D. Cashman, The transmission line antenna revisited,*IEEE Trans. Antennas and Propagat.*, **AP-38**, 575, 1990.
[63] J. M. Jarem, Electromagnetic field analysis of a four-wire anechoic chamber, *IEEE Trans. Antennas and Propagat.*, **AP-38**, 1835, 1990.
[64] Y. S. Yeh and K. K. Mei, "Theory of conical equiangular spiral antennas: Part I. Numerical techniques, *IEEE Trans. Antennas and Propagat.*, **AP-15**, 634, 1967.
[65] K. G. Balmain, Dipole admittance for magnetoplasma diagnostics, *IEEE Trans. Antennas and Propagat.*, **AP-17**, 389, 1969.
[66] B. D. Popovi'c, M. B. Dragovi'c and A. R. Djordjevi'c, *Analysis and Synthesis of Wire Antennas*, Research Studies Press, New York, 1982.
[67] B. P. Sinha and S. A. Saoudy, Rigorous analysis of finite length insulated antenna in air, *IEEE Trans. Antennas and Propagat.*, **AP-38**, 1253, 1990.
[68] G. J. Burke, *A Model for Insulated Wires in the Method of Moments Code NEC*, Lawrence Livermore National Laboratory, Rept. UCID-21301, January 1988.
[69] J. R. Wait and W. A. Pope, "The characteristics of a vertical antenna with a radial conductor ground system," *Appl. Sci. Res.*, Sec. B., Vol. 4. 177, 1954.
[70] R. W. P. King and G. S. Smith, *Antennas in Matter*, The MIT Press, Cambridge, MA, 1981.
[71] J. R. Wait, "Electromagnetic Wave Propagation Along a Buried Insulated Wire," *Canadian J. of Phys.*, Vol. 50, pp. 2402-2409, 1972.
[72] S. Bhattacharya, S. A. Long, and D. R. Wilton, The input impedance of a monopole antenna mounted on a cubical conducting box, *IEEE Trans. Antennas and Propagat.*, **AP-35**, 756, 1987.
[73] S. J. Kubina, "Measurement and computer simulation of antennas on ships and aircraft for results of operational reliability," *NATO AGARD Lecture Series No. 165*, 1989.
[74] W. Imbriale, V. Galindo-Israel and Y. Rahmat-Samii, "Numerical and experimental results of multi-wire junction tricot knit mesh reflectors by Fourier moment methods," Proceedings of 5th Annual Review of Progress in Applied Computational Electromagnetics, Monterey, CA, 692, 1989.
[75] G. H. Brown and O. M. Woodward, "Experimentally Determined Impedance Characteristics of Cylindrical Antennas," *Proceedings of the I. R. E.*, pp. 257-262, April 1945.
[76] G. J. Burke and E. K. Miller, "Modeling Antennas Near to and Penetrating a Lossy Interface," *IEEE Trans. Antennas and Propagation*, Vol. AP-**32**, pp. 1040-1049, 1984.
[77] K. R. Demarest, E. K. Miller, K. Kalbasi, and L-K Wu , "Using Model-Based Parameter Estimation for Computing Green's Functions", *IEEE Transactions on Magnetics* ,**25**, 2878, 1989
[78] G. J. Burke, E. K. Miller, S. Chakrabarti, and K. R. Demarest , "Reducing the

Number of Frequency Samples Needed to Estimate an Electromagnetic Transfer Function", *IEEE Transactions on Magnetics*,**25** 2807, 1989.
[79] E. K. Miller, "Some applications of model-based parameter estimation in computational electromagnetics, *NATO AGARD Lecture Series No. 165*, 1989.
[80] E. K. Miller and J. A. Landt, "Direct Time-Domain Techniques for Transient Radiation and Scattering from Wires", Invited Paper in *Proceedings of the IEEE*, **68**, pp. 1396-1423, 1980.
[81]. R. M. Bevensee and E. K. Miller, "The LLNL electromagnetic transient facility: design, test, and applications of a time-domain, ground-plane facility," in *Time-Domain Measurements in Electromagnetics*, E. K. Miller, ed., Van Nostrand Reinhold, New York, 1986.
[82] E. K. Miller, Editor of *"Time-Domain Measurements in Electromagnetics"*, Van Nostrand Reinhold, New York, NY, 1986.
[83] K. W. Kark and R. Dill, "A general theory on the graphical representation of antenna-radiation fields," *IEEE Trans. Antennas and Propagation*, Vol. AP-**38**, 160, 1990.
[84] J. G. Maloney, G. S. Smith and W. R. Scott, Jr., "Accurate computation of the radiation from simple antennas using the finite-difference time-domain method, *IEEE Trans. Antennas and Propagation*, Vol. AP-**38**, pp. 1059, 1990.
[85] B. J. Strait, editor, *Applications of the Method of Moments to Electromagnetic Fields*, the SCEEE Press, St. Could, Florida, 1980.
[86] B. J. Strait, and A. T. Adams, On contributions at Syracuse University to the Moment Method, *IEEE Trans. Electromagn. Comp.*, **EMC-22**, 228-237, 1980.
[87] W. L. Stutzman and G. A. Thiele , *Antenna Theory and Design*, John Wiley and Sons, New York, 1981.
[88] J. Perine, and D. J. Buchanan, Assessment of MoM Techniques for shipboard applications, *IEEE Trans. Electromagn. Comp.*, **EMC-24,** 32-39, 1982.
[89] J. Moore and R. Pizer, *"Moment Methods in Electromagnetics: Techniques and Applications"*, Wiley & Sons, New York, 1984.
[90] M. M. Ney, Method of moments as applied to electromagnetic problems, *IEEE Trans. Microwave Theory Tech.*, **MTT-33,** 972-1980, 1985.

FIGURE CAPTIONS

Fig. 1. Convergence of the admittance, Y, and impedance, Z, of a two-wavelength, center-fed dipole antenna as a function of the number of unknowns. Because the frequency is near a resonance, the admittance exhibits a smooth, monotonic behavior whereas the impedance does not, giving a quite different impression of how well-converged the model might be for a given number of unknowns.

Fig. 2. Tumble-average radar cross section of several different wire objects as a function of the sampling density/wavelength [47]. Although displaying different convergence rates for smaller sampling densities, eventually all objects approach a similar slope on this log-linear plot, indicating that the solution error decreases approximately as $\exp(-KX_S)$.

Fig. 3. Plot of tangential electric field boundary error versus position on one-half of a straight wire.

Fig. 4. Comparison of convergence rates of several different numerical methods for modeling a straight wire as a function of the number of unknowns [55]. Quantity of the ordinate is the RMS error in the current, computed on a 12-wavelength long straight wire illuminated from broadside by a planewave, for the number of unknowns on the abscissa, relative to a reference RMS current obtained for at least 250 unknowns. Models use: A) Pocklington IE with 3-term basis and point matching; B) Pocklington IE with 2-term sinusoidal basis and testing functions; C) mixed potential IE with 2-term linear basis and testing functions; and D) Pocklington IE with pulse basis and point matching.

Fig. 5. Potential and flux contours for a 90° wedge at potential V near a conducting plane at zero potential [48]. Variation of fields in vicinity of gap shows the potential difficulty of defining voltage across gap from single sample of the field.

Fig. 6. Comparison of the input impedance for a dipole antenna obtained using a local tangential electric-field source with that which results from connecting the antenna to a two-wire transmission [55]. The downward frequency shit exhibited by the transmission line results is evidently due to the capacitive loading effect of the antenna-transmission line junction.

Fig. 7. Radiation pattern of a foreshortened 19-element log-periodic antenna [55]. The antenna size is decreased by inserting inductive loads on each of the four longest elements to reduce their resonance frequencies to those that would occur if the unloaded elements were used.

Fig. 8. Comparison of the current distribution on a conical spiral antenna as obtained using an electric-field and Hallen-type integral equation [55], [64]. Even though the two results are in excellent agreement, the analytical difficulty of generalizing the Hallen approach for arbitrary wire geometries has restricted its application.

Fig. 9. Input impedance of a dipole antenna in a lossy infinite plasma. Results from the integral-equation model are in good agreement with analytical values [65], validating the numerical model's applicability to loss media. This capability is needed for the general interface problem where part or all of an antenna may be buried in a lossy ground.

Fig. 10. Input admittance of an insulated dipole antenna in air with length L, radius a = L/640 and sheath radius b = 5.84a. The relative permittivity of the sheath is 2.3 and the conductivity is zero [8].

Fig. 11. Input admittance of an insulated antenna of half-length h as a function of frequency for a sheath of relative permittivity 9 and a sheath radius b = 9a [67].

Fig. 12. (a) A computer plot of a representative monopole-screen geometry. (b) Elevation (θ) and (c) azimuth (φ with $\theta = 45^{o}$) plane patterns for 1-3 screen wires with a dipole included for comparison [55]. The total included angle of the screen wires is 30^{o}, their length is 3.0 m as is the monopole height and height above ground is 0.3 m. Results are shown for constant input power.

Fig. 13. Variation of the input impedance of a wire monopole as a function of ground-stake length [23]. This computation requires both the fields reflected from and transmitted through the air-ground interface.

Fig. 14. Input impedance of a quarter-wave monopole on a buried radial wire ground screen with N wires, showing the difference from the impedance with a perfectly conducting ground ground plane [8]. The NEC results (points) are compared with results obtained from the compensation theorem [69].

Fig. 15. Resistance of an elevated dipole due a buried wire with wire burial depth a parameter [23]. The wires are parallel to each other and the interface with their centers in a common vertical plane. Wire lengths are L = 0.125 and diameters 0.0002, with elevated dipole 0.02 above the interface, all distances measured in free-space wavelength.

Fig. 16. Propagation constant on an insulated wire at a depth d below an interface computed with Sommerfeld integral approach in NEC [23] (the dots and x's) and independent solution [71], the lines. The upper half space is air, the complex relative permittivity of the medium surrounding the wire $10 - j10^{4}$ and the insulation is air. Wire radius $a = 2.38 \times 10^{-7}$ free-space wavelengths, sheath radius b = 3a, and $\beta_0 = 2\pi/\lambda_0$.

Fig. 17. Results for monopole antenna mounted at edge of conducting box, with the patch geometry (a) and comparison of computed and measured results (b) [72].

Fig. 18. Wire-grid model of P-3/CP-140 aircraft (a) and comparison of measured and computed results for input impedance of short-wire antenna as a function of frequency (b) [73].

Fig. 19. Some results comparing predicted and measured transmission loss of two models of mesh reflector [74]. The results on the left are for a "perfect" mesh having good electrical connections at the nodes and on the right for a mesh with broken connections.

Fig. 20. Current on a quarter-wave monopole excited by a 1 V source at its base, comparing results incorporating endcap correction on the right, and using the thin-wire kernel on the left [8].

Fig. 21. Transmitted component in the air of the radial Sommerfeld field due to a vertical current source 0.1 free-space wavelength beneath the interface for a ground of relative permittivity 16 [23], as modeled by least squares approximation. A total of 88 points are fit to the rigorously computed Sommerfeld integral (36 in the plane of the figure with the visible ones shown).

Fig. 22. Input admittance of a forked monopole (monopole with vee end, one arm slightly different in length from the other) on a perfectly conducting ground. Directly computed values (————) are compared with MBPE rational-function results (------), employing n = 4 and d = 4, based on the eight samples indicated by the dots [78],[79].

Fig. 23. Comparison of the computed and measured results for the short-circuit current excited on a monopole antenna and the corresponding frequency response [81].

Fig. 24. Wire-grid truck model over perfect ground (a) yields input admittance (b) from time-domain integral-equation [55]. Results approximate the behavior of a CB antenna connected to rear bumper of light utility vehicle.

Fig. 25. Demonstration of nonlinear time-domain model of dipole (1 m long) which conducts current in only one direction [55]. The model incorporates 60 ideal diodes and exhibits possibility of pulse shaping using such loads. Feedpoint current (a) produces initial radiated pulse (b) due to Gaussian exciting voltage at center while second pulse is caused by stopping of the charge as it reaches the dipole ends, resulting in a notched spectrum (c).

Fig. 26. One frame from a set showing field-pattern motion near a nonsymmetrical biconical antenna fed in the TEM-mode [83]. The antenna is one wavelength in radius.

Fig. 27. One frame from a set showing radiation of a Gaussian pulse from a conical monopole antenna [84]. The gray scale plots show the magnitude of the electric field, the line drawing shows the surface charge density on the antenna.

F. 1

WHILE IMPEDANCE RESULTS MAY IMPLY THAT POOR CONVERGENCE IS OBTAINED--

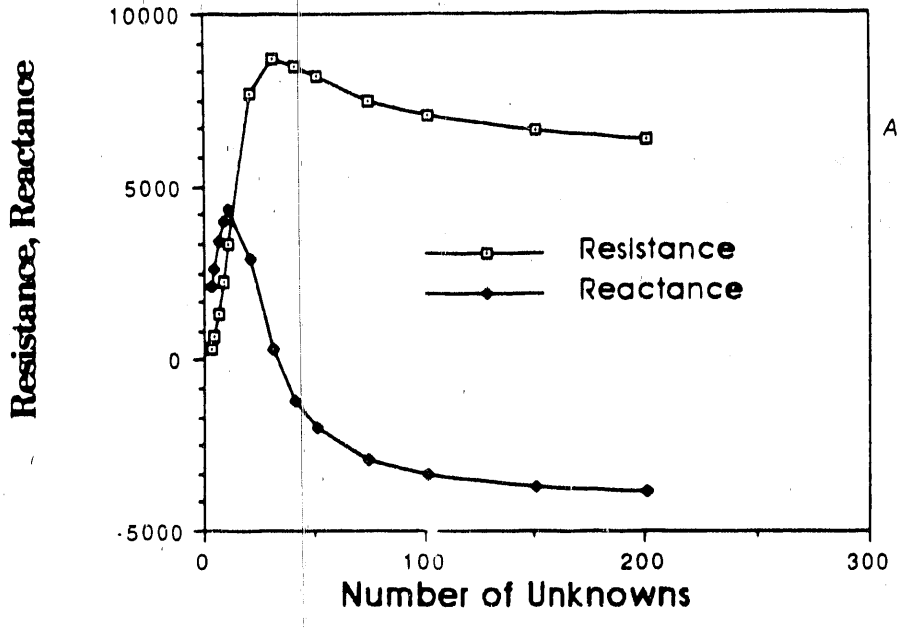

--THE ADMITTANCE REVEALS THAT GOOD CONVERGENCE IS ACTUALLY ACHIEVED

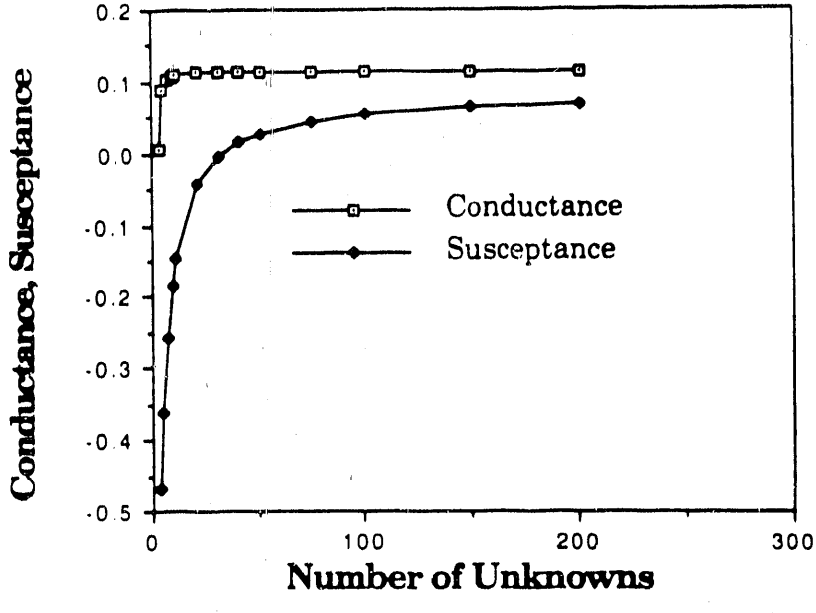

F. 2

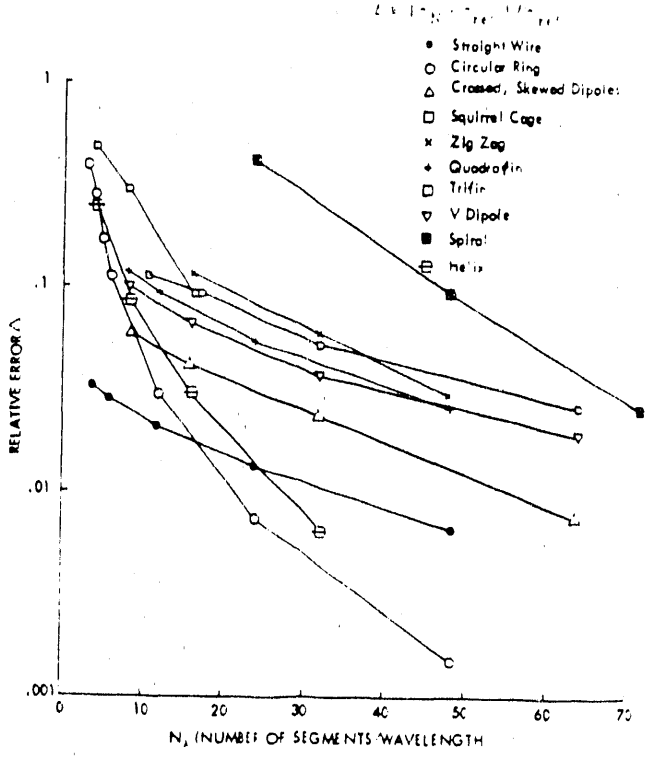

Fig. 2. Relative error as function of number of segments per wavelength.

F. 3

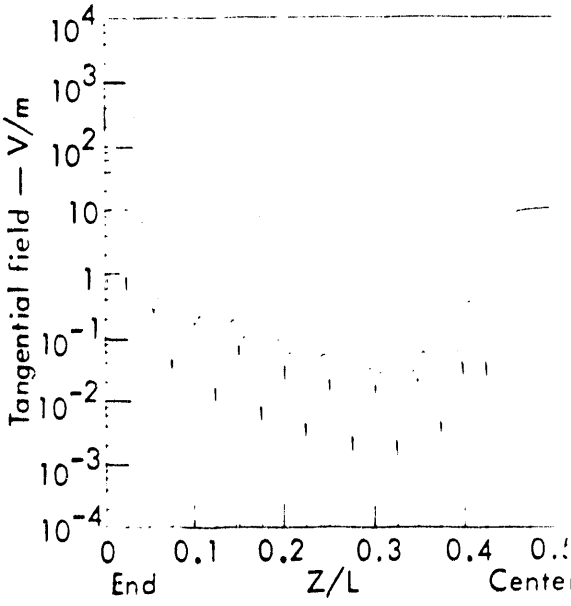

Fig. 3. Three-term sinusoidal with junction slope and amplitude matching in the antenna and field source cases (~~WF-MBA-LLL2A1~~).

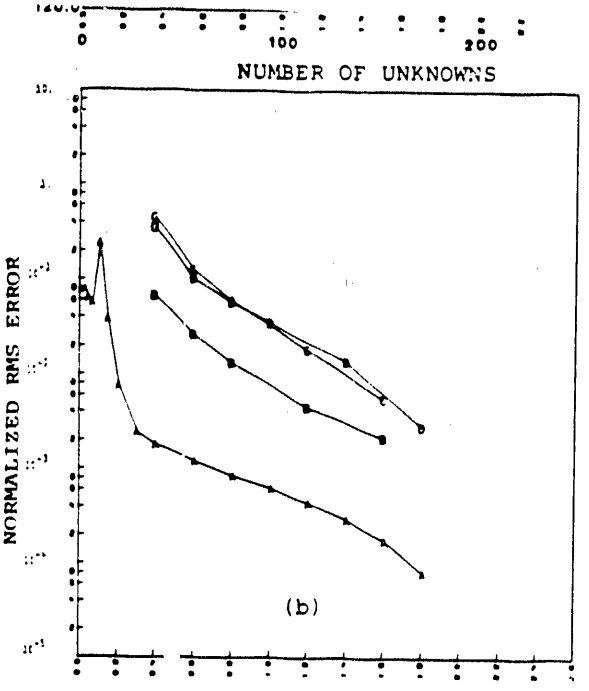

F. 4

Fig. 1. Convergence rate for several numerical methods [10]. Quantity on the ordinate in (a) is the normalized RMS current and in (b) the RMS error in current for the number of unknowns on the abscissa, relative to a reference RMS current obtained for $N = N_R \geq 250$. Results are for a straight wire of length $L \cong 12\ \lambda$ long illuminated from broadside by a planewave. Numerical models employed are as described in the references listed.

F.5

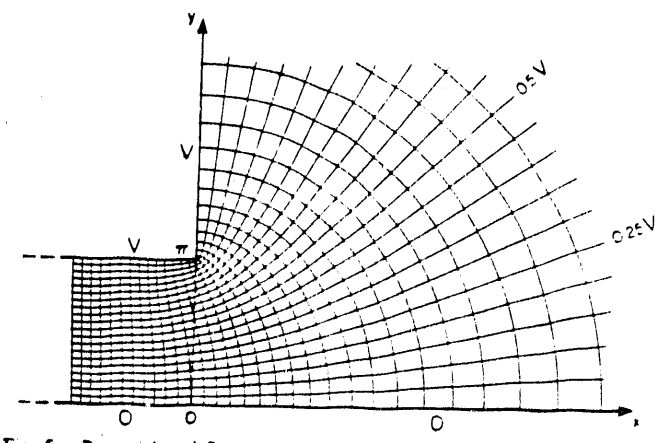

Fig. 5. Potential and flux contours for the limiting case of a 90° wedge at potential V near a plane at zero potential

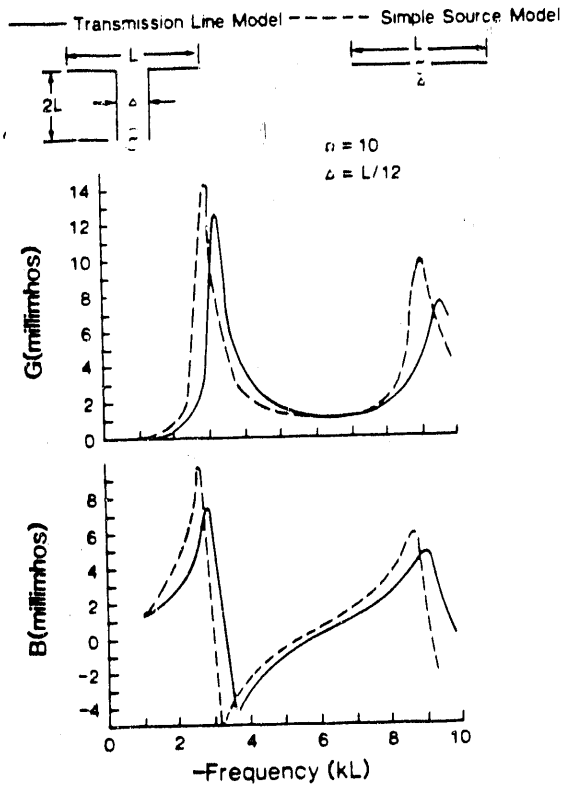

Fig. 4. Comparison of the input impedance for a dipole antenna obtained using a tangential electric-field source with that which results from connecting the antenna to a two-wire transmission line. The downward frequency shift exhibited by the transmission line results is evidently due to the capacitive loading effect of the antenna-transmission line junction.

F. 6

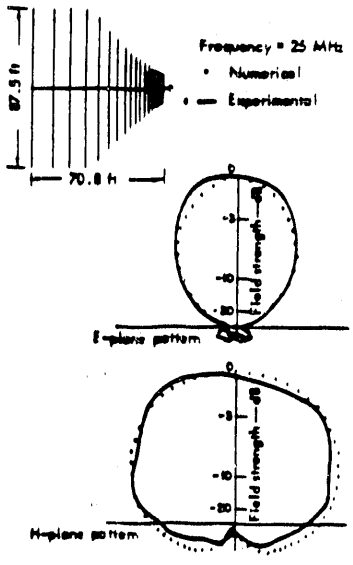

Fig. 11. Radiation pattern of a foreshortened 19-element log-periodic antenna. The antenna size is decreased by inserting inductive loads on each of the four longest elements to reduce their resonance frequencies to those that would occur if the unloaded elements were used.

F. 7

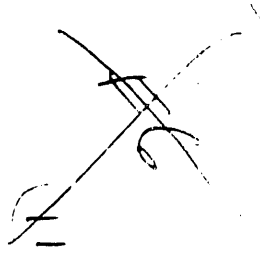

F 8

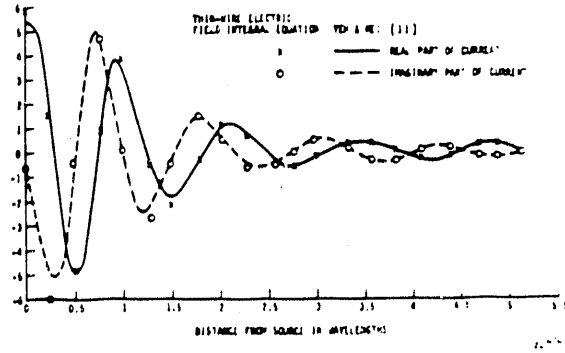

'ig. 10. Comparison of the current
listribution on a conical spiral
intenna as obtained using an electric-
field and Hallen-type integral equations
[50]. Even though the two results are
in excellent agreement, the analytical
difficulty of generalizing the Hallen
approach for arbitrary wire geometries
has restricted its application.

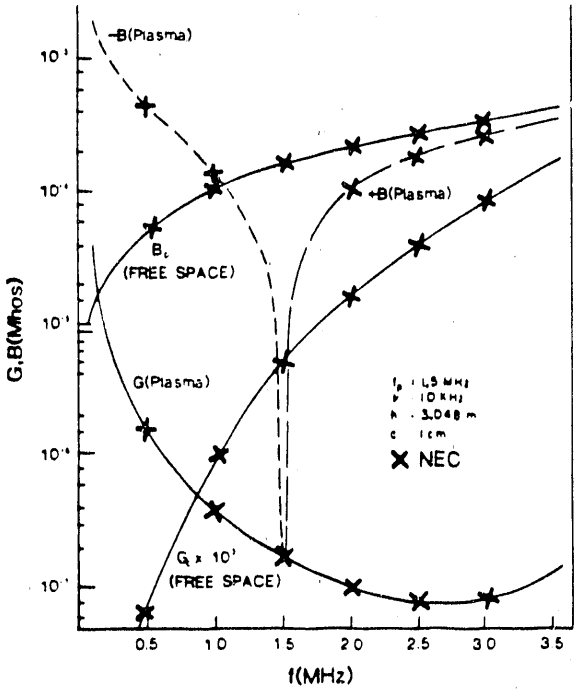

Fig. 7. Input impedance of a dipole antenna in a lossy infinite plasma. Results from the integral-equation model are in good agreement with analytical values [54], validating the numerical model's applicability to lossy media. This capability is needed for the general interface problem where part or all of an antenna may be buried in a lossy ground.

F. 9

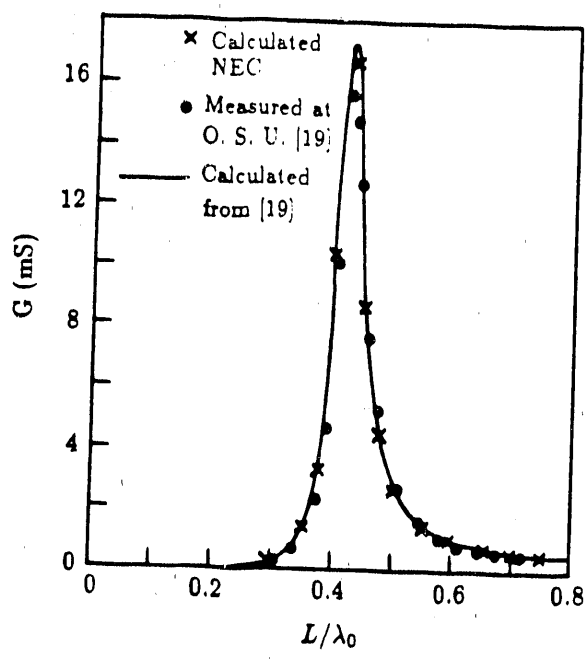
× Calculated NEC
• Measured at O. S. U. [19]
Calculated from [19]
G (mS)
16
12
8
4
0
0
0.2
0.4
0.6
0.8
L/λ_0

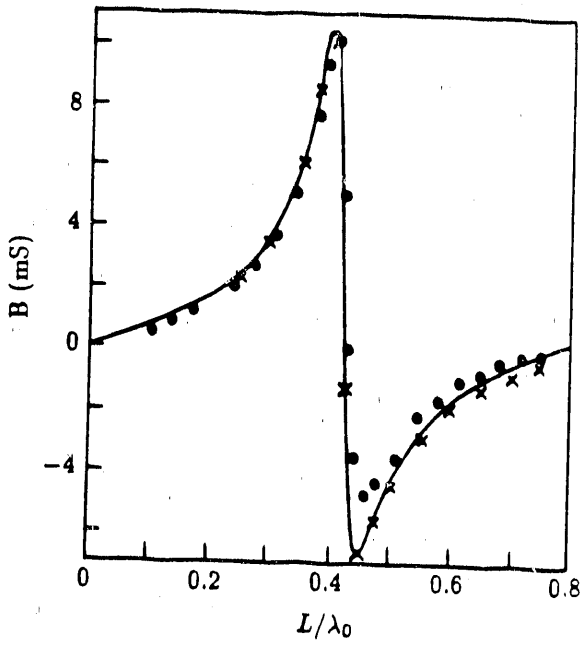
B (mS)
8
4
0
−4
0
0.2
0.4
0.6
0.8
L/λ_0

F. 10

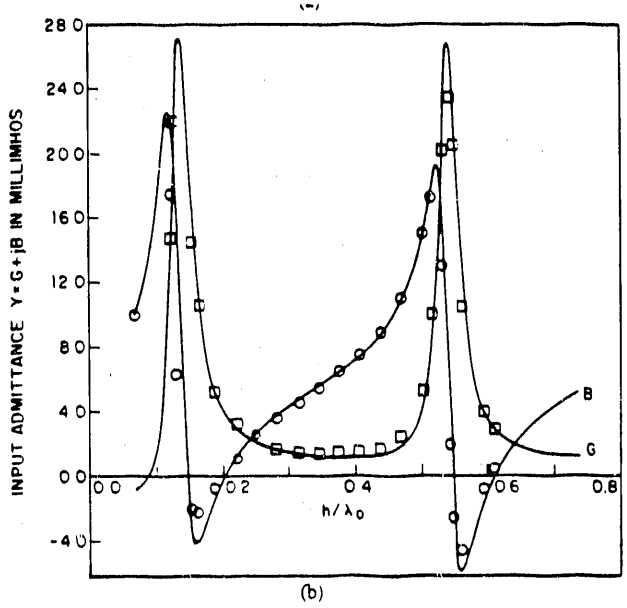

(b)

Fig. 3. Input admittance of an insulated antenna for (a) $\epsilon_r = 3.2$, $b/a = 2$ and (b) $\epsilon_r = 9$, $b/a = 4$.

F. 11

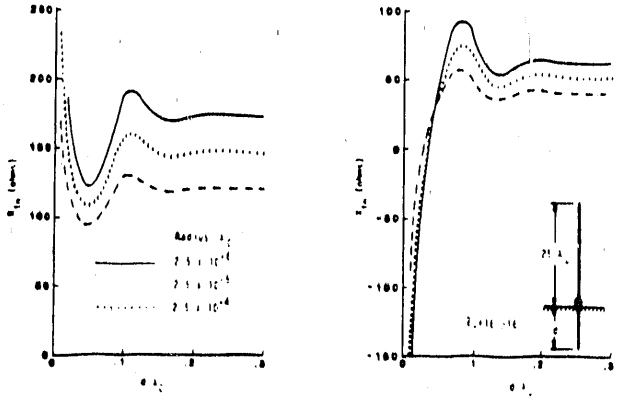

Fig. 28. Variation of the input impedance of a wire monopole as a function of ground-stake length [60]. This computation requires both the fields reflected from and transmitted through the air-ground interface.

F.13

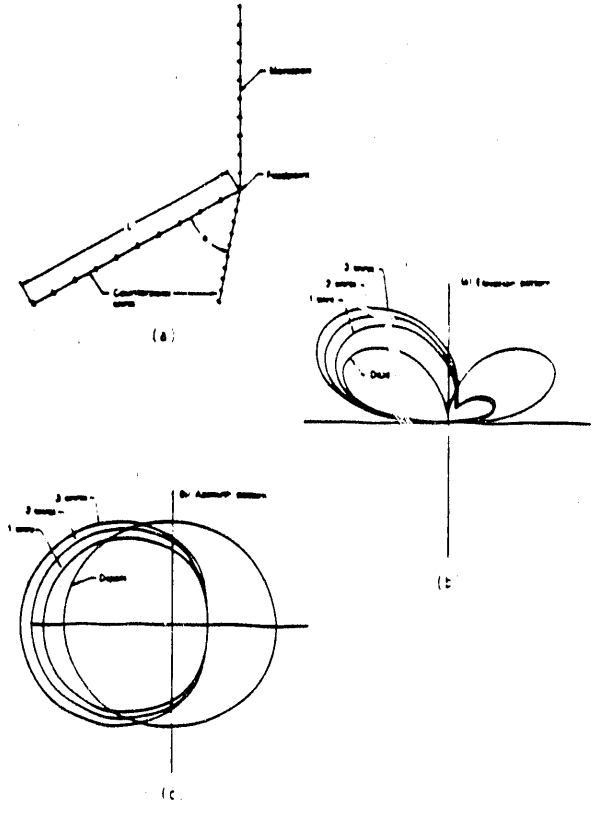

Fig. 29. (a) A computer plot of a representative monopole-screen geometry. (b) Elevation (θ) and (c) azimuth (ø with θ = 45°) plane patterns for 1-3 screen wires with a dipole included for comparison [64]. The total included angle of the screen wires is 30°, their length is 3.0 m as is the monopole height and height above ground is 0.3 m. Results shown are for constant input power.

F.12

F. 14

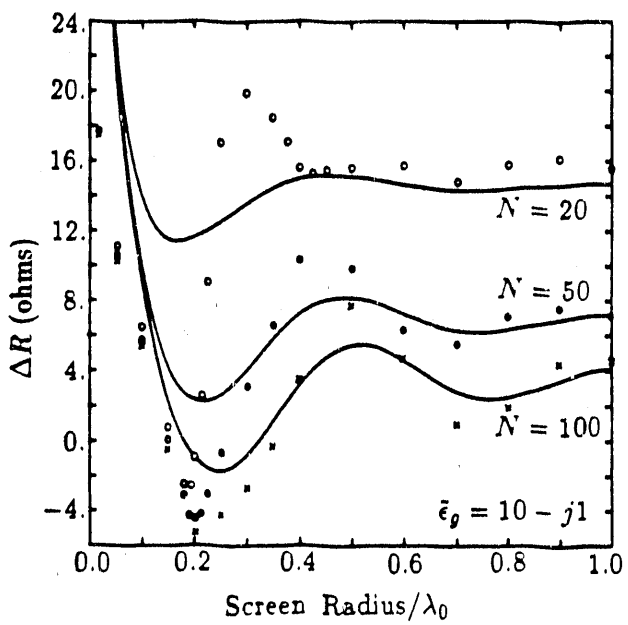
24.
20.
16.
12.
8.
4.
0.
−4.
ΔR (ohms)
N = 20
N = 50
N = 100
ε̃g = 10 − j1
0.0
0.2
0.4
0.6
0.8
1.0
Screen Radius/λ0

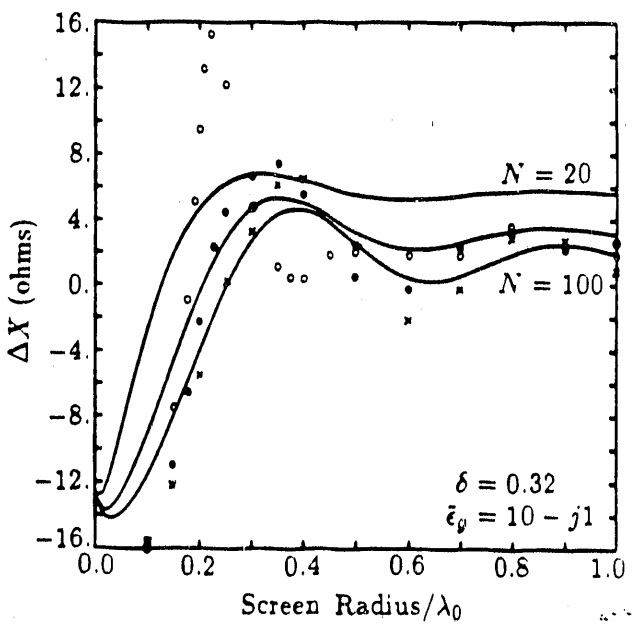
16.
12.
8.
4.
0.
−4.
−8.
−12.
−16.
ΔX (ohms)
N = 20
N = 100
δ = 0.32
ε̃g = 10 − j1
0.0
0.2
0.4
0.6
0.8
1.0
Screen Radius/λ0

...nds of the pipe

F 15

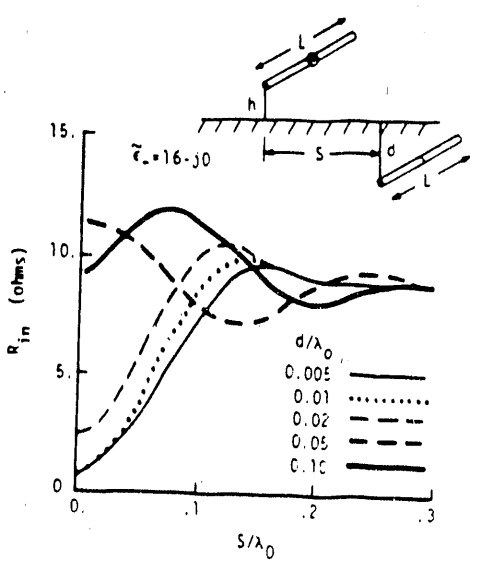

Resistance of an elevated dipole due to a buried wire with bur... a parameter. The wires are parallel to each other and the interfa...

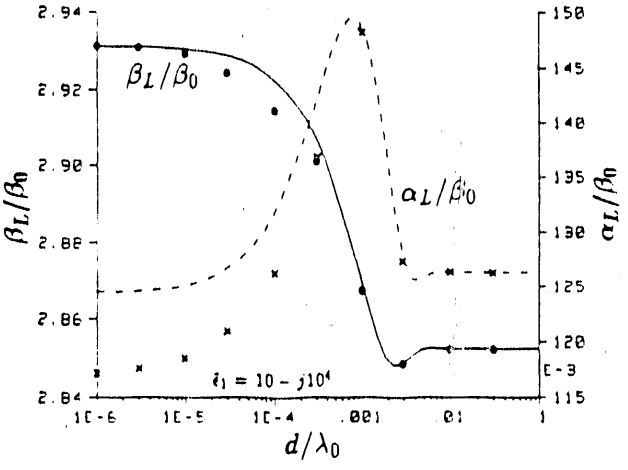
β_L/β_0
α_L/β_0
$\epsilon_1 = 10 - j10^4$
d/λ_0
2.94
2.92
2.90
2.88
2.86
2.84
150
145
140
135
130
125
120
115
E-3
1E-6
1E-5
1E-4
.001
.01
1

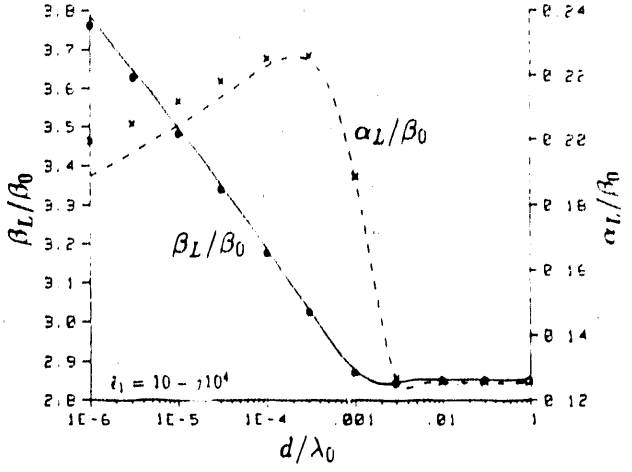
α_L/β_0
β_L/β_0
$\epsilon_1 = 10 - j10^4$
d/λ_0
3.8
3.7
3.6
3.5
3.4
3.3
3.2
3.1
3.0
2.9
2.8
1E-6
1E-5
1E-4
.001
.01
1

F 16

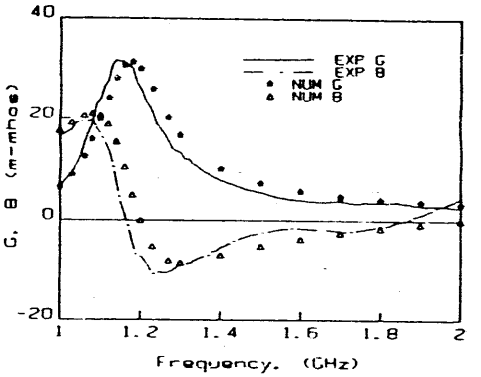

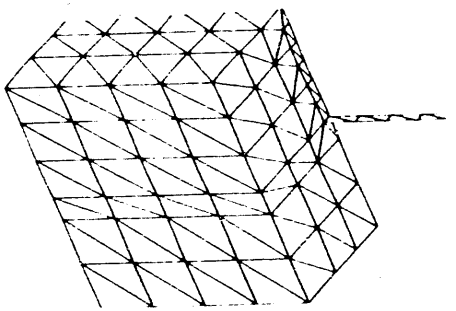

Fig. 12 Patch geometry for numerical analysis

F. 17

removed at will by numerical input. In the process of model creation it provides the medium for the creator to have better insight into the significant parameters that are important to the success of the model simulation. DIDEC is also available now for sur.

F 18a

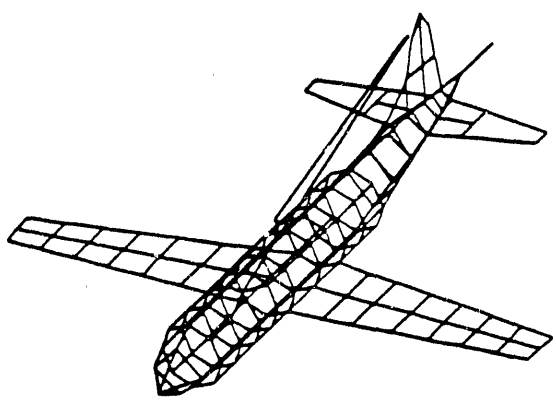

URED R

L CF R

URED X

L CF X

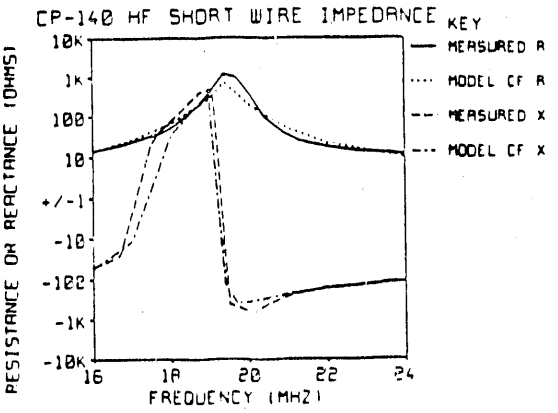

F. 18b

Figure 2.7 - Corrected Impeda

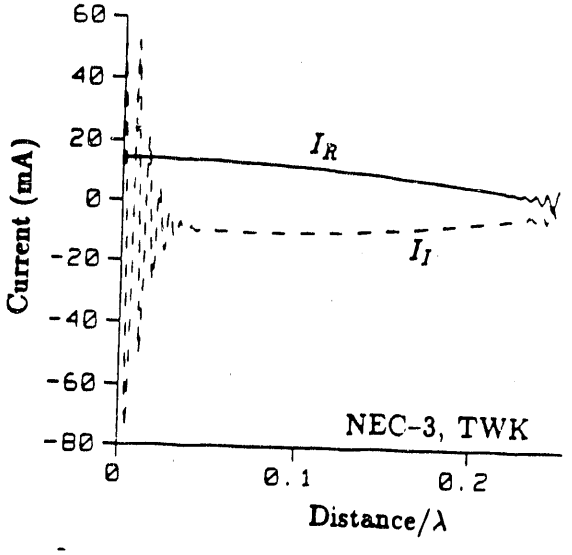
60
40
20
0
-20
-40
-60
-80
Current (mA)
I_R
I_I
NEC-3, TWK
0
0.1
0.2
Distance/λ

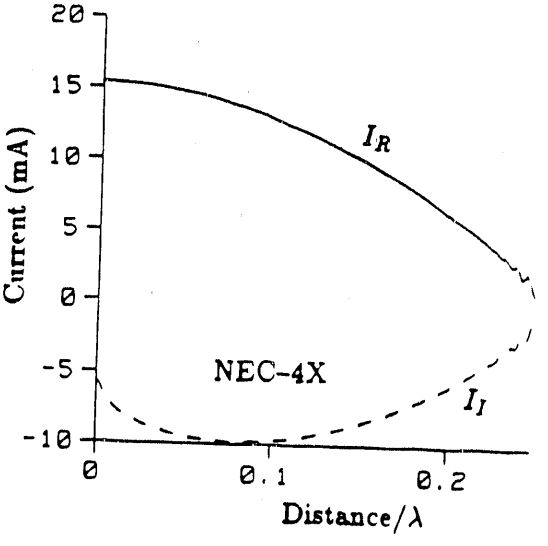
20
15
10
5
0
-5
-10
Current (mA)
I_R
NEC-4X
I_I
0
0.1
0.2
Distance/λ

F. 20

F.21

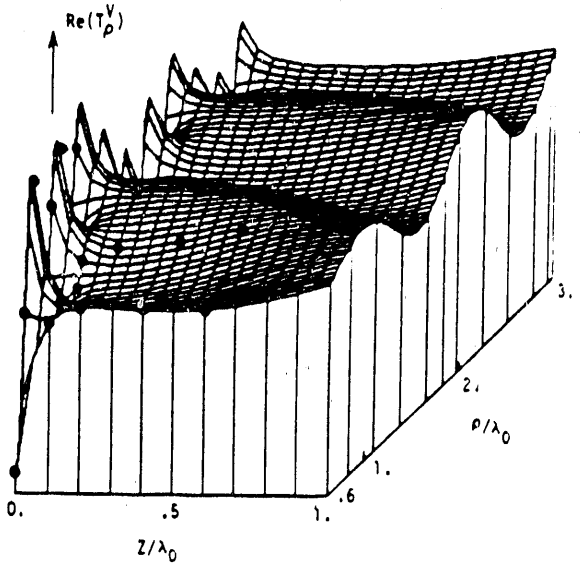

Fig 1. Transmitted field, shown for T_ρ^V component with $\tilde{\epsilon}_r = 16 - j0$ and

F.22

are compared with the rational-function model and its first derivative at the five frequencies indicated by dots.

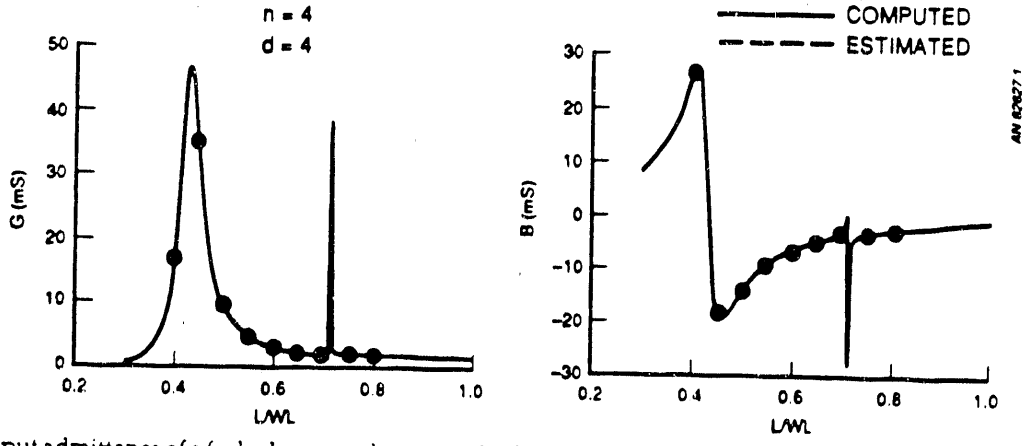

Figure 5.6. Input admittance of a forked monopole on a perfectly conducting ground. Directly computed values (_____) are compared with the rational-function model (————————) employing n = 4 and d = 4 based on the antenna admittance at the nine frequencies indicated by dots.

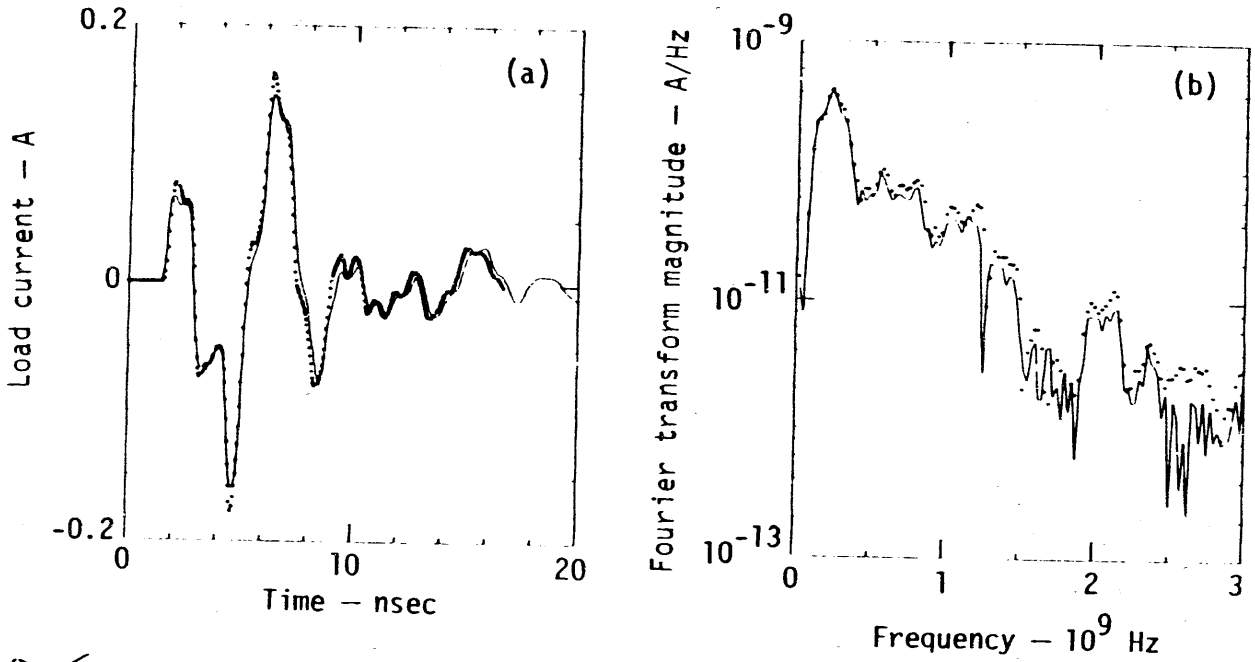

Fig. 7-5. The excellent validation of the scattered voltage measurements on the EMTF is shown by comparing, in (a), the measured short-circuit current, $I_t(t)$, in Fig. 7-2 with the current computed from the time-domain code for a 30-cm monopole on the ground plane. Their corresponding spectra also agree well in (b).

Fig 23

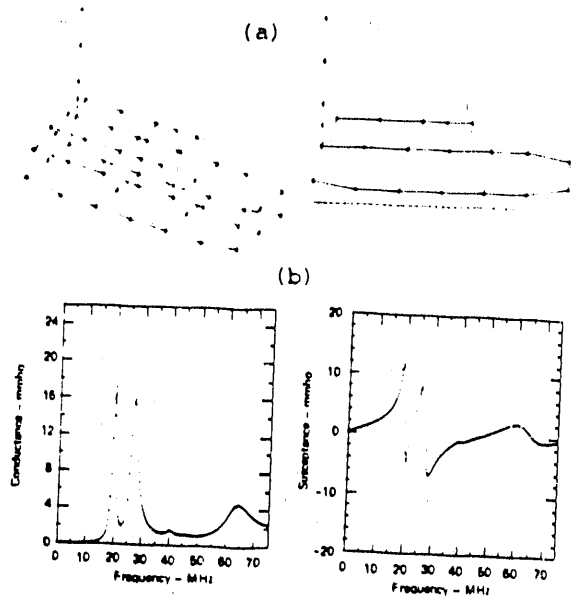

Fig. 40. Wire-grid truck model over perfect ground (a) yields input admittance (b) from time-domain calculation [49]. Results approximate the behavior of a CB antenna connected to rear bumper of light utility vehicle.

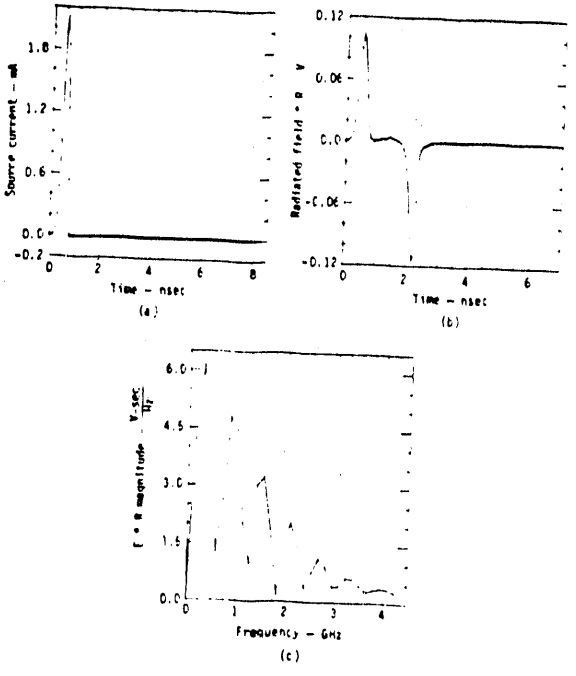

Fig. 41. Demonstration of nonlinear time-domain model of dipole (1 m long) which conducts current in only one direction. The model incorporates 60 ideal diodes and exhibits possibility of pulse shaping using such loads. Feedpoint current (a) produces initial radiated pulse (b) due to Gaussian exciting voltage at center while second pulse is caused by stopping of the charge as it reaches dipole ends, resulting in a notched spectrum (c).

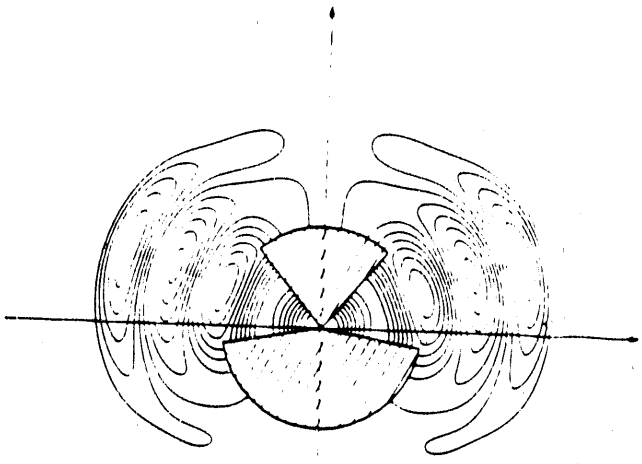

(a)

F 26

F.27

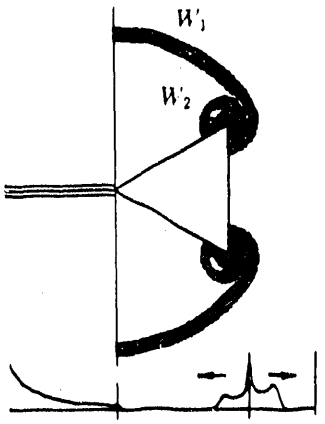

(b)

END

DATE FILMED

03 / 01 / 91